Received: 31 August 2019 | Revised: 4 February 2020 | Accepted: 23 February 2020

DOI: 10.1002/hbm.24975

RESEARCH ARTICLE

WILEY

Probing regional cortical excitability via input–output properties using transcranial magnetic stimulation and electroencephalography coupling

Estelle Raffin[1,2,3] | Sylvain Harquel[4,5] | Brice Passera[1,4] | Alan Chauvin[4,5] | Thierry Bougerol[1,4] | Olivier David[1]

[1]University of Grenoble Alpes, Inserm, U1216, Grenoble Institut Neurosciences, Grenoble, France

[2]Defitech Chair of Clinical Neuroengineering, Center for Neuroprosthetics (CNP) and Brain Mind Institute (BMI), Swiss Federal Institute of Technology (EPFL), Geneva, Switzerland

[3]Defitech Chair of Clinical Neuroengineering, Center for Neuroprosthetics (CNP) and Brain Mind Institute (BMI), Swiss Federal Institute of Technology (EPFL Valais), Clinique Romande de Réadaptation, Sion, Switzerland

[4]CNRS, UMR5105, Laboratoire Psychologie et NeuroCognition, LPNC, University of Grenoble Alpes, Grenoble, France

[5]University of Grenoble-Alpes, CNRS, CHU Grenoble Alpes, INSERM, CNRS, IRMaGe, Grenoble, France

Correspondence
Estelle Raffin, Defitech Chair of Clinical Neuroengineering, Center for Neuroprosthetics (CNP) and Brain Mind Institute (BMI), Swiss Federal Institute of Technology (EPFL), Chemin des Mines 9, 1202 Geneva, Switzerland.
Email: estelle.raffin@epfl.ch

Sylvain Harquel, LPNC—Laboratoire de Psychologie et NeuroCognition, CNRS UMR 5105—UGA, BSHM—1251 Av Centrale, CS40700, 38058 Grenoble Cedex 9, France.
Email: sylvain.harquel@univ-grenoble-alpes.fr

Funding information
France Life Imaging Network, Grant/Award Number: ANR-11-INBS-0006; NeuroCoG IDEX UGA, Grant/Award Number: ANR-15-IDEX-02; Oscilloscopus, Grant/Award Number: ANR-15-CE37-0015-01

Abstract

The modular organization of the cortex refers to subsets of highly interconnected nodes, sharing specific cytoarchitectural and dynamical properties. These properties condition the level of excitability of local pools of neurons. In this study, we described TMS evoked potentials (TEP) input–output properties to provide new insights into regional cortical excitability. We combined robotized TMS with EEG to disentangle region-specific TEP from threshold to saturation and describe their oscillatory contents. Twenty-two young healthy participants received robotized TMS pulses over the right primary motor cortex (M1), the right dorsolateral prefrontal cortex (DLPFC) and the right superior occipital lobe (SOL) at five stimulation intensities (40, 60, 80, 100, and 120% resting motor threshold) and one short-interval intracortical inhibition condition during EEG recordings. Ten additional subjects underwent the same experiment with a realistic sham TMS procedure. The results revealed interregional differences in the TEPs input–output functions as well as in the responses to paired-pulse conditioning protocols, when considering early local components (<80 ms). Each intensity in the three regions was associated with complex patterns of oscillatory activities. The quality of the regression of TEPs over stimulation intensity was used to derive a new readout for cortical excitability and dynamical properties, revealing lower excitability in the DLPFC, followed by SOL and M1. The realistic sham experiment confirmed that these early local components were not contaminated by multisensory stimulations. This study provides an entirely new analytic framework to characterize input–output relations throughout the cortex, paving the way to a more accurate definition of local cortical excitability.

KEYWORDS
cortical excitability, input–output functions, linear regression, TMS–EEG

ER and SH contributed equally to this work.

1 | INTRODUCTION

The cerebral cortex presents a modular network organization allowing better robustness, adaptivity, and evolvability of network functions (Liao, Cao, Xia, & He, 2017; Meunier, Lambiotte, & Bullmore, 2010). Some characteristics of these brain modules are strongly modulated by topological and cytoarchitectural features, including the density of pyramidal cells (Fernández-Ruiz et al., 2013), the distribution of coactivated synapses, or the architectonic configuration of the cell populations (Kajikawa & Schroeder, 2011; Murakami & Okada, 2006). The same modular system exists in the vertical direction, with a columnar organization subdivided into different layers. Each layer contains a specific distribution of neuronal cell types and connections with other cortical and subcortical regions. The differences in lamination shape the input and output connectivity of neuronal populations and delineate distinct but interconnected functional cortical areas (He et al., 2009; Meunier, Lambiotte, Fornito, Ersche, & Bullmore, 2009). This modularity of functional brain networks suggests that, at the system level, discrete cortical regions or networks are associated with specific dynamical properties, as can be defined by their input–output properties. It is indeed likely that functionally relevant nodes of a network share common input–output properties, reflecting the aggregated architecture of the subsystems components. This might form the neural bases supporting the emergence of adaptive behaviors, including sensory, motor, and cognitive functions.

Here, we refer to input–output properties as the spectrum of modulations of a cortical area's activity to varying input levels, that could either be endogenous (from another cortical area or subcortical structure) or exogenous (using external stimulation, e.g. using TMS). In all biological systems, one would expect that input–output properties follow a few regular patterns, associated with a specific physiological or behavioral phenotype. For instance, some systems are broadly sensitive, that is, the output slightly changes, either linearly or nonlinearly, over a wide range of inputs, while other systems are ultrasensitive or bistable, that is, the output characteristics vary rapidly across a narrow range of inputs (for few examples within different size scales and inputs, see, e.g., (Desmurget & Sirigu, 2012; Trebaul et al., 2018) using direct cortical stimulation in humans; (Hegerl & Juckel, 1993) using peripheral stimulation in humans; (Yi, Wang, Tsang, Wei, & Deng, 2015) using single neuron model). This dynamical and network-specific perspective on cortical physiology has been poorly or indirectly explored so far, but could provide a better estimate of the regional cortical excitability properties, characterizing the full input–output excitability profiles, from threshold to saturation.

Cortical excitability has often been ill-defined as the unidimensional cortex responsiveness to a stimulation such as TMS (Badawy, Loetscher, Macdonell, & Brodtmann, 2013) or galvanic stimulation of the contralateral median nerve (Salustri et al., 2007). Furthermore, it is usually derived from specific peripheral readouts such as motor evoked potentials (MEPs) and generalized to the whole cortex, assuming the cortex has homogeneous input–output properties (Boroojerdi, Battaglia, Muellbacher, & Cohen, 2001; Möller, Arai, Lücke, & Ziemann, 2009; Ridding & Rothwell, 1997). However, there is increasing evidence discrediting this hypothesis, as the response to different stimulation intensities appears to vary with (a) neuron types, (b) neuron circuits, and at larger scale (c) distant connectivity (Chervyakov, Sinitsyn, & Piradov, 2016; Doron & Brecht, 2015). When recording TEPs, one can directly and noninvasively assess cortical reactivity and network properties that are specific to different cortical areas (Casali, Casarotto, Rosanova, Mariotti, & Massimini, 2010; Chung, Rogasch, Hoy, & Fitzgerald, 2015; Komssi & Kähkönen, 2006; Rogasch & Fitzgerald, 2013). In a previous paper, we examined the local EEG source activity surrounding 18 different cortical TMS sites and identified region-specific spectral and spatial properties in the EEG response pattern to TMS (Harquel et al., 2016). These data, together with previous TMS–EEG data [Bortoletto, Veniero, Thut, & Miniussi, 2015; Fecchio et al., 2017; Hill et al., 2016; Rosanova et al., 2009], strongly support the notion that different cortical areas have heterogeneous response properties all over the cortex.

The description of input–output properties of corticomotor or nonmotor neuron populations using TMS–EEG have been sparsely done though, and led to conflicting results. In an early study conducted by Komssi, Kähkönen, and Ilmoniemi (2004), the authors reported a nonlinear intensity dependency of the peak amplitudes of the overall brain response when stimulating the left and right motor cortices (but see (Saari et al., 2018) for opposite findings). Over the prefrontal cortex, Kähkönen, Komssi, Wilenius, and Ilmoniemi (2005b) found a linear dependency of the overall response on stimulus intensity, but with different peak latencies. In the two TMS–EEG studies, the authors reported similar potential distributions for the different intensities. In the time–frequency domain, it has been shown over the primary motor cortex (M1) that increasing TMS intensities induce a progressive synchronization of alpha and beta rhythm in both hemispheres (Fuggetta, Fiaschi, & Manganotti, 2005). Further data also showed that depending on the motor output (presence or absence of MEPs), the prestimulation EEG spectral power (Ferreri, Vecchio, Ponzo, Pasqualetti, & Rossini, 2014) and the interregional connectivity (Petrichella, Johnson, & He, 2017) differ. Additionally, this set of earlier papers revealed that evoked responses can be elicited even at subthreshold intensities (e.g., a minimal threshold of 60% resting motor threshold [rMT] was found by Komssi et al. to evoke a measurable brain activity over M1) although with different waveforms of overall activity (Kähkönen, Komssi, Wilenius, & Ilmoniemi, 2005a; Komssi et al., 2004; Komssi, Savolainen, Heiskala, & Kähkönen, 2007).

Paired-pulse TMS–EEG can also provide information on the local intracortical circuitry mediating inhibitory activity (Daskalakis et al., 2008; Farzan et al., 2009; Ferreri et al., 2011; Opie, Rogasch, Goldsworthy, Ridding, & Semmler, 2017; Rogasch, Daskalakis, & Fitzgerald, 2013; Rogasch, Daskalakis, & Fitzgerald, 2015; Ziemann, 2015). These studies used a paired-pulse paradigm called long-interval intracortical inhibition (LICI) with two pulses separated by 100–200 ms to investigate the presumed activation of cortical GABAergic interneurons. For both the primary motor and prefrontal cortices, the mean cortical evoked activity was decreased and all typical components were found to be reduced compared to a single pulse TMS–EEG. By opposition, contrasting results have been published regarding the effects of another paired-pulse protocol

called short-interval intracortical inhibition (SICI) over M1 using a 3 ms interval between the two pulses (Cash et al., 2017; Ferreri et al., 2011; Paus, Sipila, & Strafella, 2001). Although mediated by partially distinct receptors, a recent study showed similar amplitude reduction of the late TEP components induced by SICI and LICI (Premoli et al., 2018), which preclude any conclusion about the exact mechanisms of SICI over M1. Here, we probed the activation of $GABA_A$-ergic circuits over M1 by comparing it to single pulse TMS of different intensities and compared SICI modulations in three different brain regions.

Finally, a comprehensive definition of cortical excitability must consider the large interindividual variability in evoked neural responses, as increasingly reported in the literature (Gaspar, Rousselet, & Pernet, 2011). This variability undeniably limits the strength of the conclusions drawn from grand average ERP components, and motivates the use of more complex analytic tools (Bridwell et al., 2018), as we implemented in this article.

Hence, to fill the gap in the definition of cortical excitability, we provide a new dynamical and network perspective by characterizing the dynamical modes of the local source activity (LSA) evoked by TMS of increasing intensities in three distinct brain regions. We expected distinctive regional dynamical signatures with increasing intensities, potentially reflecting the recruitment of distinct neuronal populations. To consider the intersubject variability in ERP components, we also compared the quality of the linear regressions of the local evoked potentials on single trials. Its modulation through increasing stimulation intensities allows us to explore the sensitivity of the evoked neural activity across stimulation intensities and extract a new excitability threshold.

2 | METHODS

2.1 | Participants

Thirty healthy volunteers (19 males, aged 26.3 ± 6.2, two left handed) participated in the study. A first group of 22 subjects were recruited for the actual TMS–EEG experiment, while a second group of 10 subjects (including two participants from the first group) underwent a control experiment, in which a "realistic" sham procedure was used (see Conde et al., 2019; Gordon et al., 2018). All of them gave their written consent and filled a pre inclusion questionnaire screening for any contraindication for MRI nor TMS (Rossini et al., 2015). None had history of neurologic or psychiatric disorders, neither history of alcohol or substance abuse. All were free of any medicinal treatment likely to modulate their excitability. All participants received payment for their participation in the study. This study was approved by the ethical committee of Grenoble University Hospital (ID RCB: 2013-A01734-41), and registered on ClinicalTrials.gov (number NCT02168413).

2.2 | Protocol design

MRI and TMS acquisitions were performed at IRMaGe MRI and neurophysiology facilities (Grenoble, France). Prior to the TMS EEG experiment, we recorded cerebral anatomical T1-weighted MRI (Achieva 3.0T TX, Philips, Netherlands; T1TF2, TR = 25 ms, TE = 4 ms, voxel size = 0.95 mm^3 anisotropic). The T1 MRI was segmented in the TMS neuronavigation software (Localite GmbH, Germany) and cortical targets were defined using the standard Montreal Neurological Institute referential: right dorsolateral prefrontal cortex (DLPFC, [42;42;30] mm), right superior occipital lobe (SOL, [25;−87;33] mm) and projected on the anatomical MRI using SPM8 software inverse spatial transform. The right primary motor cortex (M1, [36;−33;64]) mm) target was located using anatomical landmark (*hand knob* of the precentral gyrus) and readjusted on the hotspot location to maximize EMG responses from the first dorsal interosseous (FDI) (bottom part of Figure 1).

The TMS–EEG experiment was performed in a 2-hr session. First, we prepared the subject for EEG (EEG cap setup) and we performed the coregistration step between the MRI and the physical subject's space that is necessary for the neuronavigation system. Second, a robotized hotspot hunting procedure was performed on a 7×7 grid (spaced by 7 m). The hotspot was defined as the cortical target maximizing muscular contractions from the FDI. The rMT was then assessed on the hotspot. Finally, we stimulated the three cortical areas at five different stimulation intensities (40, 60, 80, 100, 120% rMT, corresponding to 24 ± 4, 36 ± 6, 48 ± 8, 59 ± 10, 71 ± 11% of maximal stimulation output [MSO], respectively) and one paired pulse SICI protocol (conditioning pulse 80% rMT, stimulus pulse 120% rMT). The order of stimulation sites was randomized across subjects and within each site, the order of the intensities was randomized but kept constant across sites. Participants had to sit still and relax during the measurements with their eyes open while staring at a black cross in front of them.

In order to take into account the last recommendations in the TMS–EEG field, an additional control experiment was run on 10 subjects (Belardinelli et al., 2019; Conde et al., 2019). None of them were naïve to TMS and TMS–EEG experiments: two of them underwent the actual TMS–EEG experiment described above, while the remaining eight took part in other on-going studies running in the lab. The purpose of this control experiment was to provide a "realistic" sham, combining both auditory and somatosensory confounds (realSHAM). We electrically stimulated the right frontal area above right DLPFC, while placing the placebo coil on this latter target. Five different stimulation intensities were used and delivered using the same procedure previously described. rMTs were taken from previous TMS–EEG experiments undergone by these participants (40, 60, 80, 100, 120% rMT corresponding to 22 ± 5, 33 ± 8, 44 ± 9, 55 ± 11, 65 ± 14% MSO, respectively). An anecdotal evidence was found toward an absence of difference between the rMTs of the two groups (Bayesian independent *t* test, $BF_{10} = 0.6$, see Section 2.11).

2.3 | TMS parameters

Biphasic TMS pulses induced an anteroposterior followed by posteroanterior current in the brain (AP-PA) using a MagPro Cool B65-RO

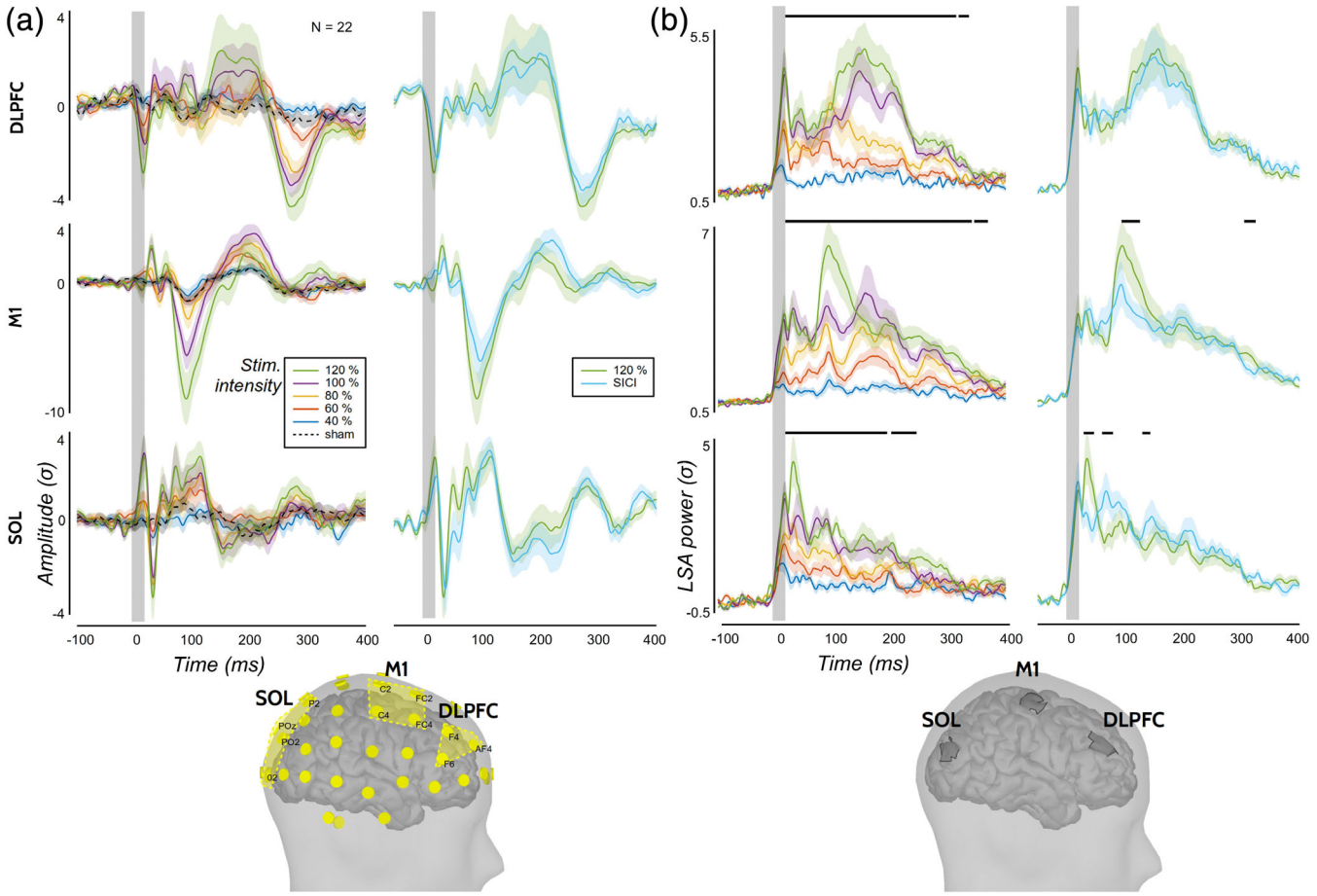

FIGURE 1 Local TMS evoked potentials (TEPs) (a) and local source activity (LSA) power (b) for each stimulation site (lines) modulated by increased stimulation intensities (colors): from 40 to 120% resting motor threshold (rMT) and for 120% rMT and short-interval intracortical inhibition (SICI) on the left and right columns, respectively. The SICI condition corresponds to the response to the conditioned and test pulses (without substraction of/normalization to the test pulse only). Lines and shaded areas represent mean and *SEM* of local TEPs (a) and LSA power (b) z-scored against baseline. Black bars indicate periods of significant difference between conditions (see text). Bottom: Electrodes clusters taken for each site for the computing of local TEPs (left) and localization of the three scouts (regions of interest [ROIs]) defined for extracting LSA (right) in one representative participant

butterfly coil (MagVenture A/S, Denmark) plugged in a MagPro ×100 TMS stimulator (MagVenture A/S). The coil was positioned and hold by a TMS robot (Axilum Robotics, France), navigated using Localite neuronavigation software (Localite GmbH). EMG electrodes were placed in a tendon-belly montage over the FDI. MEPs were recorded using a Dantec Keypoint portable EMG recording system (Natus Medical Inc.) and a CED micro 1401 MKII recording system (Digitimer, Cambridge Electronic Design, Cambridge, UK) for the six last subjects. The rMT assessment was performed using the threshold hunting method (Awiszus, 2003) over the hotspot. The coil was positioned tangentially to the scalp surface in a posterior to anterior direction angled perpendicular to the central sulcus for M1. For the two other cortical targets, the coil was positioned perpendicular to the gyrus for DLPFC, and perpendicular to the axial plane for SOL. These angles were adjusted to the standard coil orientations used in the literature and to the mechanical constrains introduced by robot's motion (Janssen, Oostendorp, & Stegeman, 2015).

Each cortical target was stimulated at instantaneous frequency around 0.5–0.7 Hz for 2 min 30 s, resulting in an average number of 80–90 trials per stimulation point. For each cortical target, we adjusted the stimulation intensities using the Stokes formula calculating the scalp–cortex distance measured from subject's anatomical MRI (Stokes et al., 2007). We performed for each subject a classical sham condition (SHAM), which consisted of stimulations 3–5 cm over one of the cortical targets at the highest intensity used for each subject, allowing us to mimic the loudest sound generated by the TMS pulse without generating any somatosensory costimulation. We used active noise cancelation intraauricular earphones (Bose QC 20) combined with white noise to mask the TMS click susceptible to evoked auditory responses on the ongoing EEG activity [ter Braack et al., 2015]. The sound level was adjusted for each subject, so that the TMS click delivered at the loudest intensity (SICI) during the session became barely audible while the delivered sound was not loud enough to induce any discomfort. A thin layer of soft plastic was

placed on the coil surface to dampen both sensory and auditory feedbacks to the subject.

2.4 | Realistic sham stimulation parameters

The realistic sham stimulation was delivered using the MagPro Cool B65-A/P RO butterfly coil (MagVenture A/S), which is a coil originally designed to perform double-blind studies (Figure 3a). The coil was flipped on the placebo side. Concurrently to each TMS pulse, an electrical stimulation was delivered through two skin electrodes (stimulating area of 10×6 mm^2) placed on the scalp underneath the EEG cap above the DLPFC area, in a bipolar montage near electrodes AF4 and F6 (Figure 3a,b). Using this system, the electrical stimulation consists in a dissymmetric triangular monophasic pulse, with rise and fall times of 200 and 2,000 μs, respectively. The current intensity can be set from 0 to 6 mA, using a maximum voltage of 1,000 V. This intensity is adjustable by users (on an arbitrary scale from 0 to 10), and varies linearly together with the % MSO used in each experimental condition (40, 60, 80, 100, 120% rMT). The maximal intensity was defined for each subject prior to the EEG recording session. To that end, we first set the stimulator to 120% rMT, and then gradually increased the electrical stimulation intensity from 0 to 10. Subjects were asked to tell which stimulation intensity produced muscular twitches or skin sensations comparable in terms of strength, pain, or discomfort, to active TMS pulses. The selected intensity was then used throughout all the control experiment (mean 5.3 ± 3.9).

2.5 | EEG acquisition

EEG was recorded using a 64 channels TMS compatible system (BrainAmp DC amplifiers and BrainCap EEG cap, Brain Products GmbH, Germany). The EEG cap set up was done following the 10–20 standard system. Electrode impedances were adjusted and kept under 5 kΩ using conduction gel. The impedance levels were checked throughout the experiment and corrected if needed during breaks between conditions. The signal was recorded using DC mode, filtered at 500 Hz anti-aliasing low-pass filter and digitalized at 5 kHz sampling frequency. During the experiment, the Fz and Afz electrodes were used as reference and ground, respectively. Channel coordinates were individually assessed using the neuronavigation software at the end of the experiment.

2.6 | EEG preprocessing

EEG signals were processed using Fieldtrip (Oostenveld, Fries, Maris, & Schoffelen, 2011) and Brainstorm3 (Tadel, Baillet, Mosher, Pantazis, & Leahy, 2011) software, and other custom scripts written in MATLAB (The MathWorks Inc.). EEG signals were preprocessed semiautomatically based on the methodology described in Rogasch et al. (2014), for each condition (three targets, six conditions, and one sham) and each subject. First, the channels showing electrical noise (flat signal or peak-to-peak amplitude superior to 100 μV) spanning more than 15% of the trials were discarded from the analysis (on average, 1.4 ± 3.2 channels per condition). EEG signals were then epoched around the TMS pulse, using a −1 to +1 s time window of interest. TMS artifacts were discarded by cutting out the −5 to +17 ms period surrounding the TMS pulses. Two rounds of independent component analysis (ICA) were then applied in order to remove noise remaining in the signal. The first ICA suppressed the muscle artifacts, while the second ICA aimed at removing the decay artifact, ocular activity, auditory-evoked potentials, and other noise-related artifacts (Rogasch et al., 2014). Before the second ICA, the signal was spline interpolated over the −5 to +17 ms period, band-pass filtered (1–80 Hz), re-referenced using the average reference, and cleaned from bad trials (leading to a mean of 73.9 ± 9.7 trials left per condition). The ocular components were automatically identified using a threshold of 0.7 on the correlation product ρ between the spatial topographies of the components and a template of typical horizontal eye movements and blinks build from our own database by averaging over subjects. Other artifact components (decay, auditory-evoked potentials, and other noises) were detected by thresholding the z-score (above 4) of their mean activity against the prestimulus period, and by visual inspection. On average, 9 (±4.2) components were removed from the signal. Cleaned EEG time series were reconstructed using the remaining components and any isolated channel still showing remaining noise was discarded from further analysis. Time series of rejected channels were finally inferred using the activity averaged over their neighboring channels (see Harquel et al., 2016, figure 3, for an illustration of the main preprocessing steps).

Additionally, for the realistic sham data that are affected by a pronounced decay artifact, we applied a decay subtraction procedure between the two rounds of ICA (adapted from Conde et al., 2019). Briefly, this procedure consists in subtracting the best fit of a two-exponential function from each trial of each channel. We used the nlinfit() function from MATLAB to estimate the five coefficients of the following regression function: $A \times \exp(B \times x) + C \times \exp(D \times x) + E$, with x being the time series of a specific trial and channel. Since the timing of the decay varies across conditions and channels, the fitting was optimized by processing it on increasing time window widths, from 200 to 800 ms by step of 100 ms. The width minimizing the mean squared error between the actual signal and the fitting function during the whole period of interest (0–1,000 ms) was taken.

2.7 | Global mean field potentials, TEPs, and LSA

First, to assess the TMS-evoked global cortical response, the global mean field potentials (GMFPs) were computed using the following formula:

$$\mathrm{GMFP}(t) = \sqrt{\sum_i^c [(Vi(t) - V\mathrm{mean}(t))2]}.\frac{1}{C}$$

where t is time, C is the number of channels, V_i is the voltage in channel i averaged across participants, and V_{mean} is the mean of the voltage in all the channels.

Next, TEPs were computed for each target, stimulation intensity and subject by averaging the EEG signal across trials, using a baseline normalization (z-scoring) over the −200 to −5 ms period. Grand average TEP was obtained by averaging normalized TEPs across subjects.

Source reconstruction for each nonnormalized TEP was performed following the default procedure proposed in Brainstorm 3 software (Tadel et al., 2011). First, the cortex and head meshes (15,000 and 10,000 vertices, respectively) of each individual were generated using the automated MRI segmentation routine of FreeSurfer (Reuter, Schmansky, Rosas, & Fischl, 2012). The locations of EEG electrodes were coregistered on each subject's anatomical MRI. The forward model was then computed using the symmetric boundary element method developed in the open MEEG freeware, using default values for conductivity and layer thickness (Gramfort, Papadopoulo, Olivi, & Clerc, 2010). The full noise covariance matrix was then computed for each subject using the temporal concatenation of the baseline periods of all conditions. Sources orientation was kept orthogonally to the cortical surface and sources amplitude was estimated using the default values of the Brainstorm implementation of the whitened and depth-weighted linear L2-minimum norm solution.

In order to extract LSA power, regions of interest (ROIs) were created on each individual anatomy using a mean spatial extent of 10 cm^2, covering about 50–60 vertices of cortical mesh. LSA power was then computed for each cortical target by averaging the absolute, smoothed (using a spatial smoothing filter with full width at half maximum of 5 mm) and normalized (z-score against baseline) source activity within its corresponding ROI. Grand average LSA power was finally calculated for each stimulation site and intensity by averaging LSA power across subjects.

2.8 | LSA mode analysis

In order to disentangle the EEG response characteristics of various stimulation intensities through the identification of modes, we proceeded to a group ICA analysis over subjects for each stimulation site independently. Following the same methodology used in Harquel et al. (2016), this decomposition was performed on the signed LSA time series S_i^k of each stimulation intensity i and subject k, from −50 to +400 ms. The signed LSA time series were computed by averaging the signed and normalized source activity within each ROI (sign of sources with opposite directions were flipped before the averaging). Each group ICA was performed after the concatenation of LSA matrices along the temporal dimension (Calhoun, Liu, & Adali, 2009), leading to a group LSA matrix M, where $M_i = [S_i^1 \ldots S_i^2 \ldots S_i^K]$ for the ith row corresponding to intensity i. M is of size $[N_i\ NK]$, where N_i is the number of intensities (6), N is the number of time bins (451), and K is the number of subjects (22). The matrix M was thus decomposed into N_i (6) independent components (data dimension) using the logistic infomax ICA algorithm (Bell & Sejnowski, 1995) with the natural gradient feature from Amari, Cichocki, and Yang as implemented in EEGLab (Makeig, Bell, Jung, & Sejnowski, 1996).

Finally, the dynamical signature of each component was assessed in each individual by means of its time/frequency (TF) decomposition obtained using Morlet wavelet transform between 7 and 45 Hz (window width of 7 cycles, 0.5 Hz bandwidth). Individual TF power maps were normalized (z-score against baseline) and averaged across subjects.

2.9 | Linear regressions of early components of the local TEP in single trials

Different linear regression analyses were performed at the scalp level. First, the local TEPs x_i were derived for each stimulation intensity i and each subject from the corresponding TEPs by averaging the signal of the four closest electrodes to each stimulation site (Figure 1a). For sham condition, local TEPs were extracted on central electrodes C1, Cz, and C2. The local TEPs were computed from +17 to +80 ms, in order to exclusively encompass the early components of the evoked activity. Then, linear regressions of the local TEPs were performed for each site on single trials s_j extracted from the same electrodes and time window, so that:

$$s_j(t) = \beta \times x_i(t) + \varepsilon(t), t \in [-17, 80]\ \text{ms} \quad (1)$$

with (i, j) ∈ {40,60,80,100,120}% rMT, and then in a second analysis with (i, j) ∈ {80%,120%, SICI}, for each (i,j) intensity pairs. The term "paired intensities," used throughout this manuscript, refers to pairs where the intensity chosen to select a TEP matched the one used to select trials (see Figure 4c for a graphical description). In such cases, the TEP was thus computed from these same trials. For sham condition, the local TEP was regressed in its corresponding trials. Finally, the quality of the linear regression was assessed by extracting t-statistics associated with the local TEP x_i factor, for each trial, intensity pair, site, and subject. For group analysis, these scores were averaged across trials for each intensity pair, site, and subject.

2.10 | Linearly scaled TEPs (simulated data)

We generated a set of simulated data whose components are linearly scaled with stimulation intensities in order to rule out a simple scaling effect of evoked temporal or spectral components. The set of simulated data $\hat{s}_i(t)$ were generated on a −400 to +600 ms period for each intensity (Figure 4b). The effect of the stimulation intensity consisted in a simple scaling of its inherent components' amplitudes, mimicking what is usually observed when increasing intensities on sensory evoked potentials (Juckel, Csépe, Molnár, Hegerl, & Karmos, 1996; Shiga et al., 2016; Tsuji, Lüders, Dinner, Lesser, & Klem, 1984). Waveform of simulated signals was designed to get close of what is typically reported in TEPs (Farzan et al., 2016), that is, from two to six alternative components together with some oscillatory patterns. Since the sole aim of these simulated data was to test the amplitude-scaling hypothesis mentioned above, the level of complexity of our simulation

was kept rather low. Simulated signals were composed of two evoked early components (positive and negative peaks p_1 and p_2) within the first 80 ms and a late induced oscillatory activity o, contaminated with noise ε drawn for a uniform distribution filtered in the 1–80 Hz frequency band:

$$\hat{s}_i(t) = A_i \times (p_1(t) - 2 \times p_2(t) + o(t)) + \varepsilon(t), t \in [-400, +600]\,\text{ms} \quad (2)$$

The two early components were modeled using Gaussian functions of different mean (30 and 45 ms) and *SD* (5 and 20 ms, respectively) parameters. The late induced activity consisted in a sinusoidal function mimicking an alpha rhythm oscillation (10 Hz) starting from +150 to +350 ms. Finally, the effect of the stimulation intensity was modeled using the amplitude factor A_i. Five different intensities were modeled, where $A_i \in \{20,40,60,80,100\}$ (Figure 4b).

2.11 | Statistics

Statistical analyses were conducted using the Fieldtrip and MATLAB statistical toolboxes on EEG signal, and using JASP Team (2018) (Version 0.9) for the Bayesian statistics analysis of regression quality scores.

2.12 | Local source activity

For each stimulation site, significant differences in the LSA across stimulation intensities were assessed over time, from +17 to +400 ms, using nonparametric permutation tests. The effect at the sample level was evaluated using the dependent samples F-statistics and T-statistics for the comparison of all stimulation intensities and the comparison between the SICI and 120% condition, respectively. The significance probability was then inferred using Monte-Carlo procedure with 10,000 permutations. Finally, *p*-values were temporally corrected for multiple comparisons: differences were considered as significant at $p < .05$ for at least 20 consecutive time bins (20 ms, see Blair & Karniski, 1993; Carota et al., 2010; Harquel et al., 2016). Statistical significance of TF maps of ICA components was obtained using paired comparisons against baseline. A nonparametric Wilcoxon test was performed per time–frequency bin, and the resulting *p*-values were spatiotemporally corrected: differences were considered significant for $p < .05$ for at least five consecutive frequency bins and 20 time bins (tiles of 2.5 Hz × 20 ms).

2.13 | Regression quality scores

The mean regression quality scores across trials were analyzed using the Bayesian equivalent of repeated measures analysis of variance (rmANOVA) and analysis of variance (ANOVA) tests. Additional post hoc analysis was performed using the Bayesian equivalent of independent and paired *t* tests. Three analyses were conducted. The first one took all data expect SHAM and SICI conditions as inputs, and performed an ANOVA with three fixed factors: TEPs' stimulation intensity, single trials' stimulation intensity, and stimulation site (including active sites and realSHAM). Subjects were included as a random factor. Then, a second ANOVA analysis focused on the regression scores obtained in paired intensities (e.g., when the TEP of 80% rMT was regressed in its corresponding trials of 80% rMT, see above) using all data (including SHAM or SICI condition), with two fixed factors: stimulation intensity and stimulation site (including active sites and realSHAM). Subjects were included as a random factor as well. Finally, a third analysis was conducted specifically on SICI, 80 and 120% rMT conditions, using a rmANOVA with three factors: TEPs' stimulation intensity, single trials' stimulation intensity and stimulation site (including only active sites). Due to the exploratory nature of this work, priors on effect sizes were kept relatively large, using default values proposed within JASP framework. Statistical evidences were reported using Bayes factors (BFs), with BF_{10} and BF_{incl} denoted the level of evidence of the alternate hypothesis (nonsigned difference) and the inclusion of a specific factor in ANOVA and rmANOVA models (across all possible models), respectively. The cut-off values, defined by Jeffreys (1998) were used to interpret BFs.

3 | RESULTS

Overall, the 22 participants tolerated well the experiment. For two subjects, however, the SICI condition over the DLPFC was too painful, and was therefore omitted. The 10 additional subjects recruited for the realistic sham experiment did not report any adverse effect. However, three of them reported an increase of the pain throughout the procedure, probably due to the cumulative effect of the electrical stimulation on the skin. Below, different aspects of the input/output properties are described through complementary features computed for each targeted cortical area.

3.1 | TEPs and GMFPs

Figure 1a presents the grand average of local TEPs for each condition and cortical site, which were obtained by averaging the EEG signal within the three or four closest electrodes to each stimulation site. Figure 2 shows the GMFP of the single pulse TMS conditions and the associated topoplots (2a) and the GMFP of the conditioned TEP (SICI) compared to the unconditioned TEP (120% stimulation intensity) with the associated topoplots (2b). Finally, TEPs and GMFPs from the realistic sham conditions are presented in Figure 3. Globally, while active conditions generated both early and late components that presented either local or distributed topographies, realistic sham conditions mostly evoked late components that were focused in the central area. The maximal voltage amplitude of early components (17–80 ms, across all electrodes) in active conditions were 2.2 ± 0.7, 2.5 ± 0.9, 3.4 ± 1.7, 4.3 ± 2.1, 6.4 ± 5.3, 7.8 ± 6.5, and 6.8 ± 3.8 μV for SHAM, 40%, 60%, 80%, 100%, 120%, and SICI condition, respectively. In contrast, the maximal voltage amplitude of early components (17 to

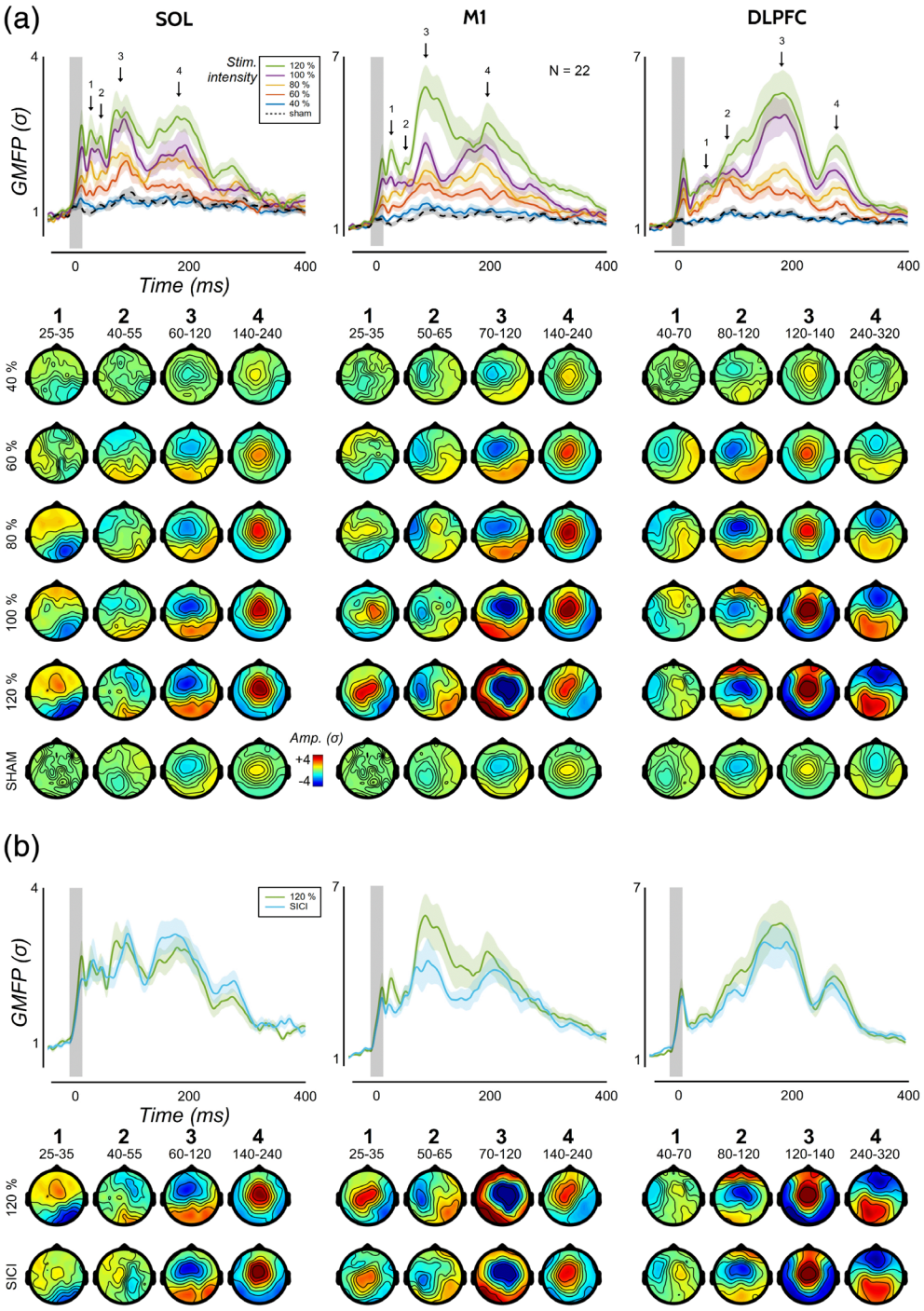

FIGURE 2 Global mean field potentials (GMFP) on active stimulations. (a) GMFP of the six single pulse TMS conditions and the associated topoplots corresponding to the four time periods displayed on top of the GMFP. Lines and shaded areas represent mean and *SE* of the GMFP z-scored against baseline. (b) GMFP of the conditioned TMS evoked potential (TEP) (short-interval intracortical inhibition [SICI]) compared to the unconditioned TEP (120% stimulation intensity) and the associated topoplots

80 ms, across all electrodes) in realistic sham conditions were 1.4 ± 0.3, 1.8 ± 0.5, 1.8 ± 0.5, 2.1 ± 0.6, and 2.5 ± 0.8 μV for 40, 60, 80, 100, and 120% stimulation intensities. Finally, the distribution of the electrical fields differed across stimulation sites, both in terms of spatial and temporal features.

3.2 | LSA power

Sources of TEPs for the three stimulated regions were estimated and local cortical responses (LSA) were extracted from the mean source time series of an ROI, centered on the stimulation target (Harquel et al., 2016). Figure 1b shows the LSA over M1, DLPFC, and SOL associated with different stimulation intensities, extracted from the clusters depicted in the bottom panel. All three regions showed a general increase of the EEG activity as a function of stimulation intensity. The strong main effect of stimulation intensity in the three regions ($p < .05$, *F*-test corrected for multiple comparisons) shows that EEG response to TMS depends on intensity for a period of at least 300 ms over M1 and DLPFC, and 250 ms for SOL. Interestingly, the three regions returned distinct local activity patterns and different activity response to stimulation intensity. While a few components showed a

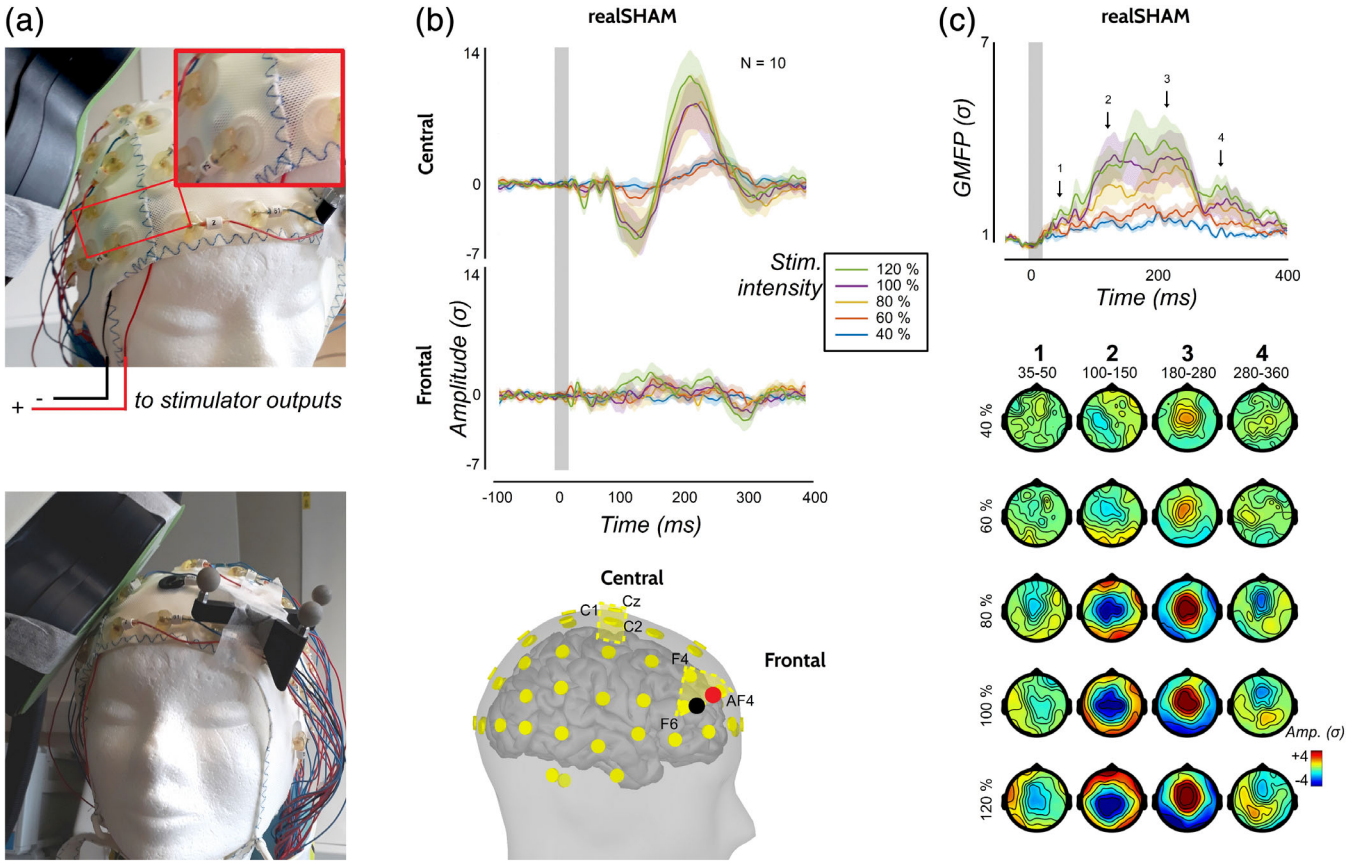

FIGURE 3 Experimental setup and results from realistic sham experiment. (a) Experimental setup for the realistic sham experiment. Electrical stimulation electrodes are placed underneath the EEG scalp nearby the dorsolateral prefrontal cortex (DLPFC) location, next to AF4 and F6 electrodes, and connected to stimulator outputs (top). The double TMS coil is then positioned over the DLPFC target, on its placebo side (bottom). (b; top): Central (top) and frontal (bottom) TMS evoked potentials (TEPs) modulated by increased stimulation intensities (colors). Lines and shaded areas represent mean and *SEM* of TEPs z-scored against baseline. (b; bottom): Electrodes clusters taken for computing of central and frontal TEPs (yellow). The location of skin electrodes used for delivering electrical stimulation is represented in black and red. (c) Global mean field potential (GMFP) of the six realistic sham conditions and the associated topoplots corresponding to the four time periods displayed on top of the GMFP. Lines and shaded areas represent mean and *SE* of the GMFP z-scored against baseline

clear linear relationship with increased intensities, for example, in M1 at 100 ms and in SOL at 30 ms, other components displayed nonlinear associations demonstrating a saturation effect already at 100% rMT, for example, late components (100–200 ms) for the DLPFC or early component (30 ms) in M1.

The LSA response patterns to SICI also differed in the three regions (right part of Figure 3b). In M1, late activities (100 and 300 ms) were significantly inhibited by SICI ($p < .05$, t test corrected for multiple comparisons) as compared with the LSA over the same region obtained with a stimulation intensity of 120% rMT. In contrast, SICI induced significant modulations on the early components: facilitation at 60 ms and inhibition at 30 ms for SOL. Interestingly, the global LSA recorded over DLPFC was not modulated by SICI. No modulation was found over the DLPFC, the SICI and the 120% rMT: LSA profiles were superimposable in the 400 ms time-window poststimulation.

A closer look on the individual TEPs revealed a large interindividual variability (Figure 4a). This observation and the increasing reports in the EEG literature regarding the interindividual variability in evoked potentials (see, e.g., Bridwell et al., 2018) prompted us to design two additional analytic tools to demonstrate that condition specific effects remained despite this high interindividual variability. These analyses aimed at (a) defining the typical oscillatory signature preferentially explained by one given condition and (b) comparing the robustness of the evoked neural activity across stimulation intensities.

3.3 | Dynamic modes of LSA

Dynamic modes (i.e., evoked time series that share common temporal properties) were inferred from a group ICA on the single subject's LSA signed time series of the five intensities and SICI, for each cortical site separately (Harquel et al., 2016). The left panels of Figure 5a display the contribution of each stimulation condition on the six components extracted from the group ICAs of each condition. The right panels of Figure 5a show the spectral contents of each component (i.e., time–frequency representation of the LSA modes). The same information is provided for the simulated data on Figure 5b.

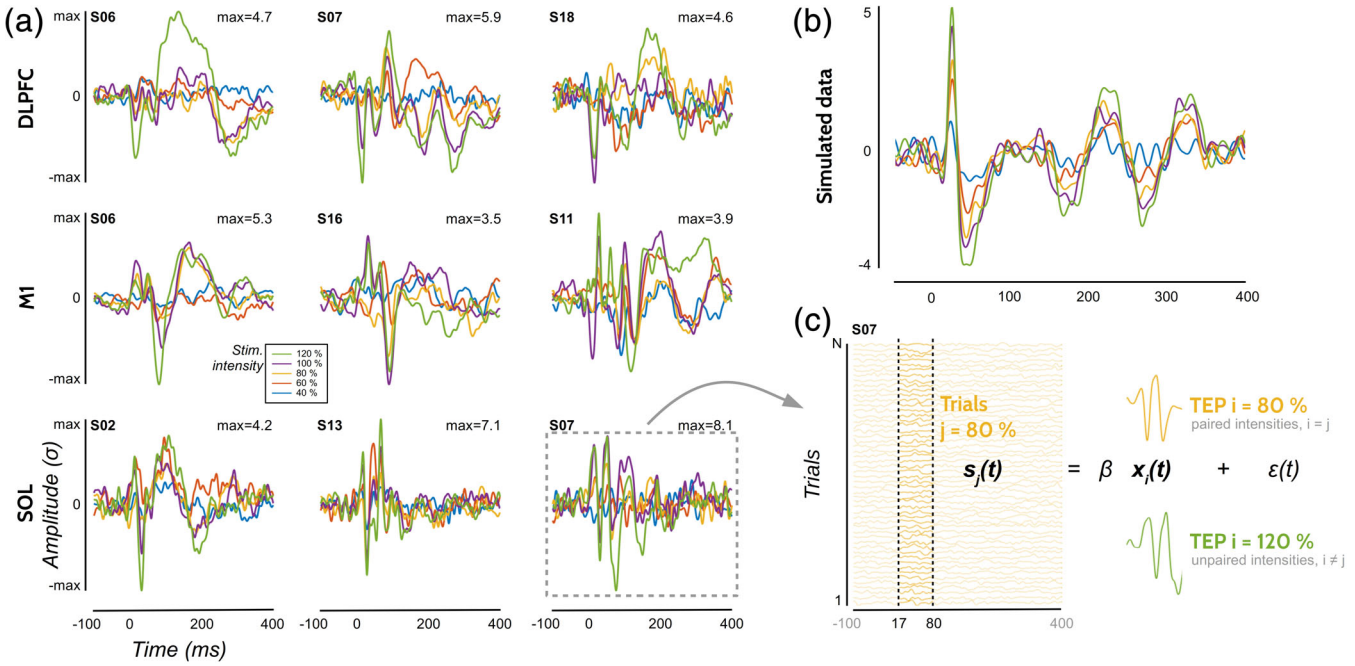

FIGURE 4 Linear regression analysis as a tool to handle interindividual variability in EEG responses to TMS. (a) Individual local TMS evoked potentials (TEPs) plotted for different subjects, for each site (rows) and stimulation intensity (colors). (b) Computed data simulating a linear scaling of the response amplitude in respect to the stimulation intensity while keeping the intrinsic dynamic. (c) Illustration of the linear regressions of the local evoked potentials on single trials

First, the explained variances of the components were somehow comparable for all physical sites (explained variance for M1 for components in increasing order: 26.9, 22.2, 20.2, 18.5, 6.8, and 5.4%, for DLPFC: 36, 21.9, 17.7, 13.3, 6.9, and 4.2% and for SOL: 29.6, 17.5, 15.7, 13.6, 12.1, and 11.3%), and each component was mainly driven by one specific stimulation condition. Only one and two components were below 10% for SOL, M1 and DLPFC, respectively, which were mainly driven by low intensities (60 and 40% rMT).

These modes were, moreover, associated with their own dynamical signature, which combined activity in the low and high frequency bands. For instance, 120% rMT over M1 was mainly explained by Component #1, which showed the most powerful and sustained mu rhythm activation (15–25 Hz, from 50 to 200 ms after stimulation onset) (Figure 5a). Mu rhythm emerged at 60% rMT in the fifth component and was maximal for Component #1, while it was diminished for SICI (Component #4). SICI was in turn associated with strong gamma activity. Low frequency waves (alpha, 10 Hz) were present in the conditions 100% rMT, 120% rMT, and SICI. Congruently for DLPFC, each LSA mode was associated with a dominant stimulation condition. Beta activity emerged at 60%, 80%, 100%, and SICI, associated with Components #2–5. In line with the TEPs, 120% and SICI, although associated with two distinct modes were relatively close to each other, with the presence of early gamma activity. Short burst of alpha activity was present in most components and reached a maximum at 80 and 100% rMT. SOL was the cortical region that showed the most complex interactions between stimulation conditions regarding their spectral contents: Component #1 showed the common signature of SICI, 100 and 40% rMT, Component #2 of SICI and 100% rMT, and Component #3 of SICI, 100 and 80% rMT. Components #1 and #2 showed sustained alpha activity, whereas gamma band activity significantly emerged in all five main modes.

In contrast, we found that the variance of simulated data was mainly explained by one single component (explained variance on the simulated data: 92.4, 2.6, 1.7, 1.6, and 1.6%) (Figure 5b). Four to five components were needed to reach 90% of explained variance in real data, compared to only one for the simulated data. All the stimulation conditions of the simulated data shared the same dynamical signature, as depicted on the corresponding time–frequency map of Figure 5b (right panels). This signature showed the two early components, generating a powerful gamma activity, together with the late alpha oscillation, that were scaled throughout all the stimulation conditions. Since all the simulated data contained only one shared source of signal, the weights of the mixing matrix are not relevant here, and are mostly affected by computational noise coming from the limitation of this decomposition in this very particular case.

3.4 | Linear regression of the local TEP in single trials

3.4.1 | Regression quality scores in every possible intensity pairs

Next, linear regressions of the early components (<80 ms) of the local evoked potentials on their single trials were performed (Figure 6a). This analysis captures the sensitivity of the evoked neural activity across stimulation intensities, by exploring the intensity-dependent

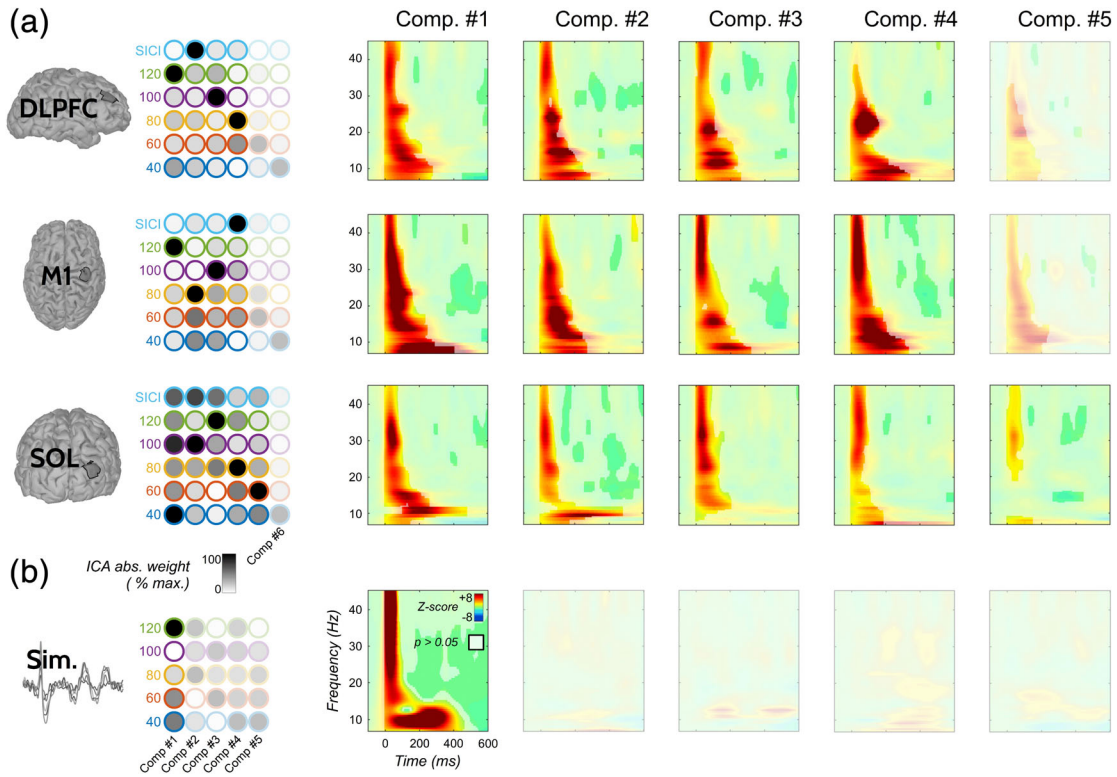

FIGURE 5 Dynamic modes of local source activity (LSA) across stimulation intensities. Left panels: Mixing matrix of group ICA for each stimulation site. For each component (in column), the relative weight of each stimulation intensity (in line and detoured using its specific color) is given by its gray scale level (from 0 in black, to 1 in white, corresponding to the maximum weight of the component). Components explaining less than 10% of total variance are masked. Right panels: Time–frequency (TF) map of each ICA component. Frequency power is normalized (z-score), and nonsignificant modulations against baseline are masked. TF maps of components explaining less than 10% of total variance are masked. (a) Real data and (b) simulated data

modulation of the quality of this regression (Figure 4c). For all conditions and sites (including active sites and realistic sham), we performed a linear regression of the TEP on individual trials at the scalp level from 17 to 80 ms. For each site, all possible combinations between TEPs and trials intensity were explored, that is, TEP 60% in 120% trials, TEP 100% in 40% trials, and so forth. The Bayesian ANOVA analysis on regression quality scores showed extreme evidence for the inclusion of all principal effects (site, TEPs intensity, and trials intensity), and all interactions between them.

First, an extreme effect of site ($BF_{incl} > 10^{13}$) was found, suggesting that the regression fit is different in the four regions (Figure 6a). Post hoc comparisons showed with strong evidence that M1 and SOL had similar fits ($BF_{10} = 0.07$), which both exceeded DLPFC (vs. M1: $BF_{10} > 500$, vs. SOL: $BF_{10} > 10^3$). All active conditions showed stronger regression quality scores than realistic sham (BF10 = 9.8; $>10^5$; $>10^7$ for DLPFC, M1, and SOL, respectively). The two other main factors (intensity of TEPs and trials) were also significant ($BF_{incl} > 10^{13}$ for both). This confirmed that the quality of the regression differed with intensity for both the TEP and the trials used for the regression, as the signal to noise ratio (SNR) gradually increased with intensity in the EEG signal.

The significant TEPs intensity by trials intensity interaction ($BF_{incl} > 10^{13}$) indicated that the regression of a given TEP fits better with the trials corresponding to the same intensity (paired intensities). Moreover, for all three active sites together, post hoc comparisons showed that the quality of regression was maximal for paired intensities (see Figure 6a), except for 40% rMT. Above 40% rMT, the best regression qualities were systematically obtained when using the same trials intensity than the TEPs intensity used for the regression (with strong to extreme evidence), confirming that each intensity has its own spatiotemporal signature. This was not the case for realistic sham conditions, where this one-to-one association was only observed in the 60 and 120% conditions (with moderate to strong evidence). Finally, a triple interaction TEPs intensity by trials intensity by site interaction ($BF_{incl} > 10^4$) showed with extreme evidence that the increase in stimulation intensity had a different impact on the regression fit in the four regions.

We conducted a complementary analysis on the regression quality scores obtained using the late components (from 80 to 400 ms) of the central evoked potentials, on C1 Cz and C2 electrodes (supplementary Figure S1). A similar Bayesian ANOVA was performed, that showed extreme evidence ($BF_{incl} > 10^{13}$) for all the three main effects and the interaction between TEPs intensity and trials intensity. However, moderate to strong evidence suggested that the interaction between site and TEPs intensity ($BF_{incl} = 0.17$), as well as the triple interaction ($BF_{incl} = 0.07$), had no effect on the model. Regarding the main effect of stimulation site, post hoc analysis revealed with strong

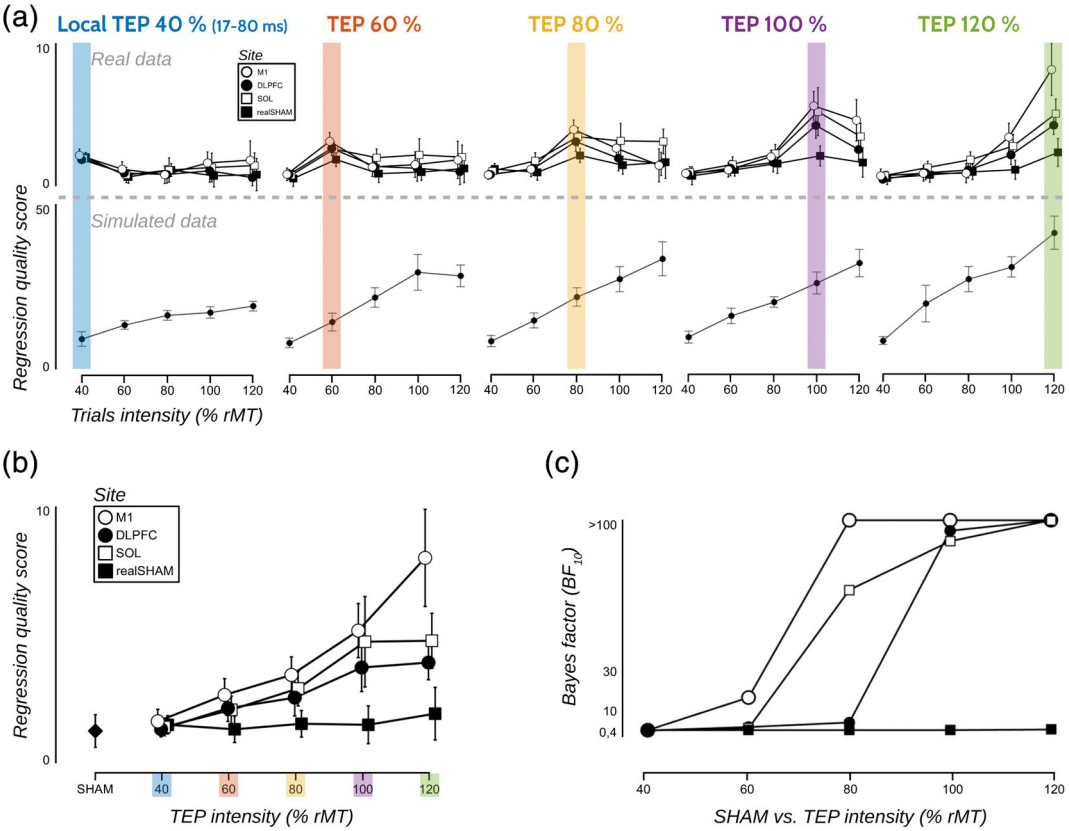

FIGURE 6 Regression quality scores modulated by increased stimulation intensities on local early components (<80 ms). (a) Regression quality scores obtained for each site (marker symbol), trials intensity (y axis), and TMS evoked potentials (TEPs) intensity (panel columns), on both real and simulated data (upper and bottom part, respectively). In each panel column, the corresponding paired intensities (where $i = j$, see Section 2) are highlighted using its specific color. (b) Regression quality scores obtained for each site in paired intensities on real data. (c) Bayes factors of post hoc comparisons between each paired intensity and SHAM condition

to extreme evidence that the quality of regression was higher on DLPFC than on M1 (BF_{10} = 27.9), SOL ($BF_{10} > 10^6$) or realistic sham (BF_{10} = 14.4). Moderate evidence showed that the quality of regression was equivalent between M1, SOL, and realistic sham (BF_{10} between 0.12 and 0.24). Unlike what we have observed with early local components, the post hoc analysis exploring the interaction between TEPs and trials intensity did not reveal any systematic better fit on paired intensities. The best fit was obtained for trials intensities that were equal to or higher than the TEP used (see Figure S1, Supporting Information). For each TEP above 40% rMT, we found extreme evidence toward differences between paired and lower intensities (all $BF_{10} > 100$), while a lack of evidence or a moderate evidence toward absences of difference emerged from the comparison between paired and higher intensities (BF_{10} between 0.17 and 1).

3.4.2 | Regression quality scores on simulated data

To demonstrate that increased intensities do not act like a simple scaling of the evoked components on real data, we generated a set of simulated data whose components were linearly scaled with stimulation intensities (see Section 2). The same statistical model applied to the simulated data showed significant main effects of TEPs intensity (BF_{incl} = +inf) and trials intensity (BF_{incl} = +inf) as well as a significant TEPs intensity by trials intensity interaction ($BF_{incl} > 10^7$). Importantly, post hoc tests revealed that the best fit was obtained with 120% rMT trials whichever TEPs intensity was used for the regression. Figure 6a shows this clear linear relationship between intensities and regression quality scores, and the difference regarding curve shape with real data.

3.4.3 | Regression quality scores in paired intensity

Next, we restricted our model to the TEPs regressed with their corresponding trials (e.g., M1 TEP 100% rMT regressed on M1 100% rMT trials), including the sham and the realistic sham conditions in the model. A Bayesian ANOVA revealed extreme main effects of TEPs intensity ($BF_{incl} > 10^{14}$), site ($BF_{incl} > 10^{11}$), and a TEPs intensity by site interaction ($BF_{incl} > 10^5$). Figure 6b shows the four different response curves associated with the four stimulation sites. Post hoc comparisons showed that a stimulation intensity effect was present for all three active sites (for M1: $BF_{10} > 10^{12}$, for DLPFC: $BF_{incl} > 10^7$, for SOL: $BF_{incl} > 10^5$),

whereas a moderate evidence toward an absence of stimulation intensity effect was found for the realistic sham conditions (BF_{incl} = 0.16).

The analysis of Figure 6b suggests a saturation effect at 100% rMT for DLPFC and SOL. Post hoc pairwise comparisons indeed provided substantial evidence for similar regression fits between 100 and 120% over DLPFC (BF_{10} = 0.23) and SOL (BF_{10} = 0.23), and moderate evidence for a better regression at 120% for M1 (BF_{10} = 6.5). They also revealed that the minimal intensity needed to reach a statistical difference with sham was 60% rMT over M1 (Figure 6c). Over the DLPFC and SOL, TMS needed to be applied at 100 and at 80% rMT, respectively, to reach strong statistical evidence. No statistical evidence was found to infer about a difference or an absence of difference between realistic sham conditions and sham, in any used intensity (all BF_{10} fell between 0.38 and 0.74, Figure 6c).

3.4.4 | Regression quality scores in SICI condition

The last rmANOVA performed on 80, 120% rMT and SICI conditions also indicated a significant TEPs intensity effect (BF_{incl} = +inf) and a significant site × TEPs intensity interaction (BF_{incl} = 9.2). Post hoc tests (Figure 7a) showed that the regression quality scores acquired with SICI were smaller than for 120% rMT only for M1 (BF_{10} = 10.6). Moderate evidence tended to show that it had no effect on the quality of the regression for DLPFC and SOL (BF_{10} = 0.25 and BF_{10} = 0.23, respectively). Considering all intensity pairs, a last analysis showed again a typical response pattern for the SICI trials (extreme TEPs intensity by trials intensity interaction: $BF_{incl} > 10^{15}$) that were better regressed by their own TEP and could not be found in the other conditions (Figure 7b). This comparison further suggests that SICI, which is composed by a first TMS pulse at 80% rMT and a second one at 120% rMT, induced a specific pattern of activity which significantly differed from single pulse TMS given at 80 or 120% rMT.

4 | DISCUSSION

In the present paper, we reported a set of new EEG markers able to quantify interregional differences in input–output properties and inhibitory activities in three different brain areas.

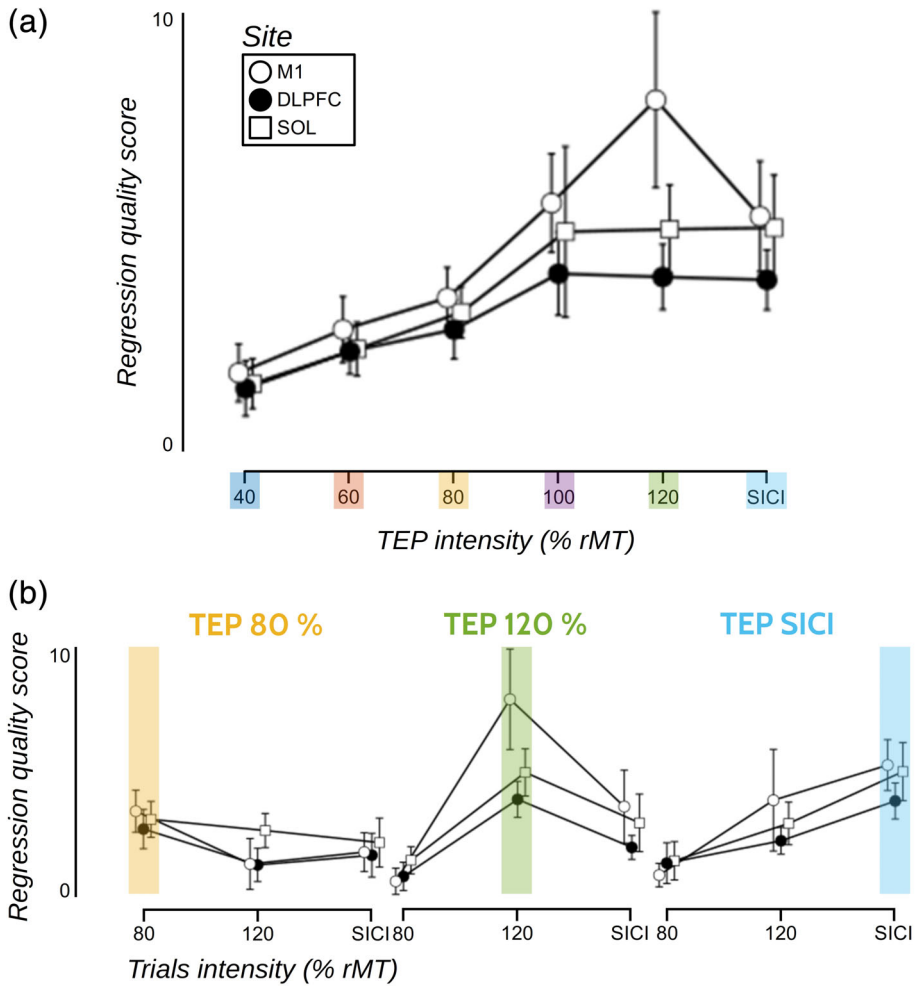

FIGURE 7 Regression quality scores modulated by short-interval intracortical inhibition (SICI). (a) Regression quality scores obtained for each site in paired intensities. (b) Regression quality scores obtained for each site, trials intensity (y axis), and TMS evoked potentials (TEPs) intensity (panel columns). In each panel column, the corresponding paired intensities (where *i* = *j*, see Section 2) are highlighted using its specific color

4.1 | Regional input output properties of the cerebral cortex

4.1.1 | Local neural activity scales with stimulation intensity

LSA recorded in the three regions with the five intensities showed an overall dose-dependency relationship. This finding replicates previous TMS–EEG or TMS–fMRI studies, either stimulating the primary motor cortex (Bohning et al., 1999; Komssi et al., 2004; Komssi et al., 2007) or the left middle frontal gyrus (Kähkönen et al., 2005a). The earlier TMS–EEG studies have intrinsic limitations in terms of data acquisition and analysis, precluding a full understanding of the input–output response function to TMS. Although ROI analyses in the source space have been criticized (Farahibozorg et al., 2018), the LSA profiles computed from each of the three ROIs encompassing the stimulated area, allowed us to distinguish complex shapes of biological input–output relationships. Unlike Komssi et al. (2004) where all EEG peaks depended nonlinearly on stimulation intensity up to 100 ms poststimulation, our patterns of changes yielded to mixed results in M1. The N100 showed a clear linear relationship while the P30 increased nonlinearly with increased stimulation intensity. This discrepancy was also present in the two other regions showing nonlinear dependencies (i.e., the N100/P200 for both the DLPFC and SOL), as well as linear dependencies (i.e., the P200 and P30 for the DLPFC and SOL, respectively).

While each EEG component reflects brain activation and is thought to be associated with one or more cognitive processes (Brandeis & Lehmann, 1986; Sur & Sinha, 2009), the exact functional meaning and cortical origin of each TEP's peaks are not clear. The electrophysiological nature of the TMS-induced EEG components is indeed difficult to interpret, since (a) EEG represents the summation of excitatory and inhibitory afferents over a large population of neurons (Kirschstein & Köhling, 2009), and (b) TMS elicits neural activation both locally and remotely with the activation of corticocortical or corticosubcortical loops (Bortoletto et al., 2015; Rogasch & Fitzgerald, 2013; Siebner, Conde, Tomasevic, Thielscher, & Bergmann, 2019). However, we know that the amplitude of this TMS-evoked response relays information on the excitability and reactivity of the underlying cortical networks, as the amplitude of the peaks and troughs are sensitive to changes in cortical excitability (Harquel et al., 2016; Veniero, Bortoletto, & Miniussi, 2014). The dynamics of these input–output relationships can then express information about the size of the neuron population and its level of synchrony during the component generation. Therefore, the various shapes of input–output relationships of each EEG components reveal distinct local properties, in terms of synchronization properties of neuronal networks. For instance, the shorter latency components (<60 ms), which are thought to be more influenced by the physical features of the stimulus (here the TMS pulse) present a ceiling effect in M1 (no further increase in LSA between 100% rMT and 120% rMT). This might reflect saturation in synchronous activation of local neurons involved in the generation of these components.

Comparing M1 and DLPFC, Kähkönen et al. (2005b) found different reactivities of motor and prefrontal cortices and different dynamics. A quadratic polynomial function described the data of motor cortex, whereas a linear model fitted better for the response–stimulus intensity function of prefrontal TMS. We also found that the dynamic of the input/output functions differed across the three regions, suggesting different dynamical properties of neuronal responses. This provides additional evidence that TMS–EEG can noninvasively probe regional differences in cortical microcircuits underlying functional cytoarchitecture (Harquel et al., 2016). Of interest, a recent study investigated the effect of stimulation intensities of intermittent theta burst stimulation on the cortical properties assessed with TMS–EEG. The authors reported an inverse U-shaped relation between intensity and induced plastic effects, where 75% iTBS yielded the largest neurophysiological changes (Chung et al., 2018). These results not only raised interesting aspects about the relationship between intensity and plasticity induction but also about homeostatic regulation maintained through the recruitment of excitatory and inhibitory subpopulations of neurons, which can be characterized by TMS–EEG components (Premoli et al., 2014). Then, for rTMS treatments applied in "silent" regions, a systematic description of the input–output functions of different cortical areas is crucial in order to induce the most efficient plasticity change. An individual and fine-tuning of rTMS intensity is particularly important given that the brain responses to rTMS are dose dependent, precisely, stimulation intensities influences the plasticity induction (see, e.g. Nettekoven et al., 2014 or Fitzgerald et al., 2002). Using regional biophysical models of neural plasticity induced by TMS and individual input–output excitability profiles, getting more reliable rTMS outcomes might be possible. Alternatively, for clinical practices, the use of region-specific atlases of excitability profiles might already help the clinicians to define the optimal ranges of stimulation intensities, although this last option does not take into account the particularities of pathological brains.

4.1.2 | Intensity-dependent spectral properties of the evoked neuronal responses

Earlier single-pulse TMS–EEG data (Lea-Carnall, Montemurro, Trujillo-Barreto, Parkes, & El-Deredy, 2016; Rosanova et al., 2009) indicated that each brain region mostly resonates at its own natural frequency. Moreover, our previous work showed that distant cortical areas can also share common dynamical properties, depending on their local cytoarchitectonics (Harquel et al., 2016). In the primary motor cortex, Fuggetta et al. (2005) showed that different stimulation intensities appear to involve different levels of modulation of oscillatory activity. Precisely, increases in alpha and beta power were found to be more pronounced with increasing of stimulation intensity from subthreshold to the 130% rMT. Here, we used LSA modes decomposition to further reveal that different intensities in each of the tested regions were associated with distinct and complex patterns of oscillatory activities, rather than with a linear or nonlinear scaling of a specific frequency pattern.

For the three tested sites, our group ICA including the five intensities and the SICI condition revealed at least four components with comparable level of explained variances, arguing for the existence of mixed and complex dynamics. Moreover, each component was mainly driven by one unique stimulation intensity, which entails its own oscillatory signature. In addition, to explain approximately 90% of the total variance, all components have to be included, suggesting that each stimulation condition is associated with a complex mixture of oscillatory signals.

As a matter of fact, the power of the so-called "natural" rhythm of a given area was not the only one impacted by stimulation intensity. Instead, this analysis showed that the input–output relationship is unlikely to be driven by a simple linear scaling of the stimulation intensity as for the simulated data. The variance of simulated data was mainly explained by one single component (explained variance on the simulated data: 90.9, 3.5, 2.7, 1.2,and 0.78%), which means that the same information content, and its related oscillatory signature, can be found in all conditions. To sum up, this analysis demonstrated that each stimulation intensity induced oscillatory activities reflecting complex combination of frequency bands, distinct from each other and different across brain regions.

The changes observed in the EEG activity at low TMS intensity are thought to originate from the stimulation of the superficial layers of the cortex through both direct and indirect excitation of pyramidal neurons in the gray matter (Di Lazzaro et al., 2000; Kujirai et al., 1993; Ziemann, Rothwell, & Ridding, 1996). In contrast, by increasing stimulation intensities, the direct axonal pathways in deep gray matter structures get activated (Amassian & Cracco, 1987; Nakamura, Kitagawa, Kawaguchi, & Tsuji, 1996). This could additionally activate deeper subcortical structures and trigger complex corticosubcortical loops. Such indirect subcortical or transcallosal effects might also account for the change in oscillatory activity induced by stronger TMS pulses that we observed in the three regions.

4.2 | TEP linear regression quality as a new readout for input–output properties?

Classical studies investigating input–output properties of the cortex rely on group-based component analyses. Modulation of specific components at the group level (either in the temporal or spectral domain) by different experimental conditions or stimulation intensities is thought to return information about the input–output function of the cortex. However, in such analysis frameworks the interindividual variability of the evoked response regarding its dynamic characteristics is neglected. For example, the relevance of studying N45 amplitude modulations is questionable if this component is absent, reversed in terms of polarity, or delayed in several subjects (Lioumis, Kičić, Savolainen, Mäkelä, & Kähkönen, 2009). Here, we propose a different approach based on the linear regression of TEP in single trials for each subject. This method allows to fully consider the intersubject variability of the dynamics of the evoked response, since subject-specific dynamical contents of TEPs will not influence the regression process. The quality of the regression could provide a new local readout for cortical excitability and dynamical properties specificity. Precisely, cortical excitability could be defined by the quality of the regression of TEPs' early components compared across intensities for each cortical region. The rationale of this new metric is that, at similar stimulation intensities, highly excitable neural populations would be more prone to produce electrical activity above noise level in a single trial basis, compared to low-excitable populations. This will be associated with better quality of TEP regression. In the same line, inspecting the shape of the relationship between regression quality and stimulation intensity might provide a more specific definition of cortical excitability definition.

The results showed first that regression fits were overall smaller in the DLPFC compared to SOL and M1, indicating a lower excitability in this region, at least regarding early components. This means that each trial carries more information from local neural activations for M1 and SOL compared to DLPFC in which a single trial poorly explains the average TEP. A new regional cortical excitability index can then be inferred based on the comparison of the regression quality obtained in the sham condition and with different TMS intensities. This index would correspond to the weakest stimulation intensity able to elicit significant TEP regression quality (i.e., different from sham stimulation). Note that as expected, our analysis also showed that the goodness of fit gradually improves with intensity, reflecting a better SNR with increasing intensities. This metric has the advantage to be defined locally even in "silent" areas and does not rely on peripheral readout. It is biologically informative because it directly reflects the quantity of energy needed to evoke a meaningful EEG signal in a given brain region. This idea is reinforced by the fact that no significant information could have been retrieved from realistic sham conditions. As shown by the comparison between areas, it is sensitive enough to discriminate the different excitability levels between different cortical areas. The input–output curves drawn from regression score suggested that the primary motor cortex was the most excitable area (eliciting significant activity from 60% rMT), followed by SOL and DLPFC (80 and 100% rMT, respectively). Fecchio and colleagues also report larger local mean field potentials evoked over M1 compared to prefrontal, premotor, and parietal targets (Fecchio et al., 2017). This has direct consequences on TMS titration for clinical trials. Our data suggest that adjusting rTMS intensities (for instance, applied to the DLPFC) to the rMT is suboptimal. The new excitability metric we present here brings instead an accurate estimate of regional excitability, which could serve as a basis to better adjust stimulation intensities. In the same vein, Casali et al., 2010 also derived a local excitability estimate based on the minimal TMS intensity needed to significantly activate more than 1% of the cortical sources within the stimulated area, and found comparable values over the superior occipital lobe (Casali et al., 2010).

Furthermore, regression quality could also provide interesting insights about the dynamical properties of the evoked response and especially about its modulation across brain areas and stimulation intensities. Our results showed that above 40% rMT, the quality of regression is maximal for the trials corresponding to the regressed

TEP, confirming that each intensity has its own spatiotemporal signature. For example, the dynamic properties of the TEP obtained with 100% rMT could not be found on the EEG activity evoked by 80% or 120% rMT stimulations. This phenomenon was partially observed in realistic sham conditions (in 60 and 120% rMT conditions), showing that a part of this effect might originate from the specificity of the preprocessing (mostly ICAs, and decay correction for realSHAM) that was done independently on the different set of data. However, the level of regression quality in paired realistic sham conditions never differed from sham condition, showing that this spurious interaction effect can be ignored. Again, the same analysis performed on simulated data consisting in a simple scaling of the EEG response to increased TMS intensity, returned linear relationships between the quality of the regression and TMS intensities. This shows that unlike the real data, the TEP of each intensity can be found in all single trials with better fits using higher intensities. In this case then, the different intensities have similar spatiotemporal correlates. Importantly, a key challenge remains to define the precise and individual relationship between the modeling and simulation of TMS induced electrical field and the neuronal activation threshold based on EEG recordings that is relevant for therapeutic outcomes or side effects in each of the brain area.

4.3 | Regional inhibitory properties of the cerebral cortex

4.3.1 | Local neural activity shows opposite response patterns to SICI

Paired-pulse TMS delivered with an interval of 2–3 ms can noninvasively probe the level of GABAA receptor (GABAAR) mediated inhibition (Di Lazzaro et al., 2007; Kujirai et al., 1993). Importantly, the resulting EEG responses reflect the combination of the conditioning effects of the first pulse on the second one and vice versa. Then the interpretation is not as straight forward than a unique activation of GABAAR.

To our knowledge, there are only four studies investigating the EEG correlates of SICI in M1 (Cash et al., 2017; Ferreri et al., 2011; Paus et al., 2001; Premoli et al., 2018) and one in the DLPFC (Cash et al., 2017). These few studies, however, reported inconsistent results in terms of changes in components amplitude. While Paus et al. did not report any change, Ferreri et al., as well as Cash et al. found a reduction of the early components (P30, N45, and P60), and Premoli et al. found a reduction rather in the late components (N100, P180). Similarly, we found a significant reduction of the N100 and P300 compared to single pulse TMS at 120% rMT. Interestingly, SICI induced an opposite effect in the superior occipital lobule with an increase of the P60 and the N145 but a decrease in the P30 and no effect in the DLPFC. This last finding is incongruent with the results obtained by Cash et al., who found a reduction in P60. These discrepancies can be explained by different stimulation parameters (monophasic pulses vs. biphasic pulses), data analysis (here, we focused on the LSA) or study design (double sample size, or neuronavigation).

4.3.2 | Region-specific spectral properties of SICI

SICI applied over M1 induced significant oscillatory activities distinct from those induced by single pulse TMS at other intensities. SICI abolished the mu rhythm over M1, which is tightly associated with the sensorimotor system. Mu activity is suppressed during the execution of movements, representations of movements, and on activation of afferent influences associated with muscle activity (Sabate, Llanos, Enriquez, & Rodriguez, 2012). This result was thus expected, since SICI is known to level down the activation of the corticospinal track through the activation of intracortical inhibitory circuits, leading to a decrease in the induced muscle contraction. In the occipital cortex, the spectral properties of SICI were explained by a mixture of components including low gamma, alpha, and beta activity. This reflected a complex oscillatory signature mainly shared by 100 and 120% rMT conditions. In the DLPFC, the neural activity evoked by SICI stimulation shared common spectral properties with the conditions 120, 100, and 60% rMT. The spectral signature of SICI and 120% SICI were really close confirming the lack of effect of SICI on the EEG signal, associated with early broadband gamma activity and late alpha.

4.3.3 | TEP linear regression quality of SICI

When the SICI condition was included in the linear regression analysis, it overall confirmed the original dynamical signature of SICI in M1 because SICI trials were better regressed by its own TEP. When all conditions were entered, the quality of the regression was weaker for SICI than for 120% rMT only for M1. This might be due to the lesser recruitment of the neuronal populations responsible for the activation of the corticospinal tract (PYR V neurons). The fact that we did not find the same patterns of results for the two other regions, suggests that neurotransmitters density are different across regions (Tiwari, Ambadipudi, & Patel, 2013). However, in a recent pharmacological TMS–EEG study targeting M1, the authors tested two different drugs (diazepam, baclofen) sensitive to GABAAR and GABABR mediated inhibitory neurotransmission, respectively. While SICI induced an amplitude reduction of late TEP components (i.e., N100 and P180) compared to single-pulse responses, diazepam and baclofen modulated SICI of N100 in opposite directions (Premoli et al., 2018), similar to earlier findings related to LICI (Premoli et al., 2014). Because SICI has distinct impacts depending on the stimulated area, TMS–EEG could provide a new regional readout for drug testing specifically targeting GABAergic mechanisms in predefined brain areas.

4.4 | Potential experimental confounds

Our comparison of the EEG effects induced by the different intensities is inevitably confounded by TMS-induced muscular, auditory and somatosensory responses, as called peripheral evoked potentials (PEPs). Below, we will discuss how our data and our new analysis approach might add new insights concerning the contribution of these

multisensory costimulations into the TMS-induced EEG response, with respect to the classical sham procedure and the realistic sham experiment we conducted. Several recent lines of evidence suggest that realistic sham stimulation induces a cortical response pattern close to the one evoked by real TMS over the scalp [Biabani et al., 2019; Conde et al., 2019]. The current debate on this topic (Belardinelli et al., 2019; Siebner et al., 2019) prompted us to better disentangle the multisensory temporal and spatial response patterns from the real transcranial evoked brain response to TMS.

First, the TMS-induced auditory sound may have contributed to the TMS intensity-dependent changes of components' amplitude in the three tested regions, contaminating the early components (i.e., P30, P60) and the late components (i.e., the N100 and P200). Indeed, the "click" sound of TMS increases with intensity (Dhamne et al., 2014) producing an increase in AEP (Juckel et al., 1996). Additionally, intensity-dependent artifact can result from cranial muscle activity related to direct depolarization of muscle fibers by the TMS pulse or from activation of the nerves innervating the muscles (Mutanen, Mäki, & Ilmoniemi, 2013). Finally, there are additional regional sources of artifacts. For example, over M1, the presence of intensity-dependent muscle reafferent inputs to S1 induced by suprathreshold TMS over M1 results in sensory-evoked potentials in the EEG, which can contaminate the TEP (Fecchio et al., 2017). In the same line, TMS over the DLPFC can be uncomfortable and this feeling of discomfort is proportional to TMS intensity. One way to quantify the weight of these nonneuronal signals in the various TEPs would be to systematically rate the discomfort and pain induced by all the stimulation conditions and relate it to the associated TEPs.

A further development of our cortical mapping would be to systematically and online fine-tune TMS parameters (angle, intensity, position) to minimize artifacts and maximize cortical responses before starting the acquisition [see, e.g., Casarotto et al., 2016]. This approach would allow a better comparison of interregional signals and a less extensive use of postprocessing computations. However, we tried in the present work to minimize confound effects both during acquisition and EEG processing steps. First, we used a realistic sham condition consisting in a TMS sham coil able to mimic the TMS multisensory effects without directly stimulating the brain (Smith & Peterchev, 2018). We also used state-of-the-art methods to reduce the auditory component (plastic form under the coil and sound-protective headphones playing white noise). Then, we applied state-of-the-art methods to process TMS–EEG data by using the methodology developed in 2014 by Rogasch et al., which rely on systematic and meticulous data cleaning steps using two ICA rounds. Such a method allowed us to remove any residual muscular or auditory artifacts from our data, and to compute clean TEPs showing significant early neuronal activations (Belardinelli et al., 2019).

Despite all these measures, it is still impossible to dissociate the multiple sources of multisensory stimulations induced by TMS. Then the resulting input–output patterns are partly ambiguous and cannot be definitively attributed to direct local cortical TEP profiles. However, the results of our realistic sham experiment clearly stated that no significant information can be drawn locally from the early components of PEPs (<80 ms) using our methodology, contrary to its late central components. The quality of regression of the realistic sham conditions on early components never significantly differed from noise, as quantified with the classical sham procedure used in the first experiment. This is in line with recent findings suggesting that only late components appear to contain significant PEPs (Biabani et al., 2019; Freedberg et al., 2020). In contrast, recruitment curves drawn from active stimulation differed from noise and showed different patterns across sites, possibly revealing different input–output properties of the cortical tissue. Additionally, both our LSA modes and regression quality analyses enabled us to link one stimulation intensity with one specific dynamical signature, distinct from each other, which was not the case with realistic sham data. Using simulated data, we also demonstrated that these results were in contradiction with the hypothesis of a simple scaling effect of evoked temporal or spectral components, which would be the case for increasing auditory or somatosensory stimulation (Juckel et al., 1996; Shiga et al., 2016; Tsuji et al., 1984). Interestingly, this latter hypothesis is partially confirmed on late central components, since our complementary analysis revealed that no specific dynamic signature can be drawn across (or between) stimulation intensities at such latencies. However, further analyses of these components have to be performed. Several pieces of evidence, such as the different spatial and temporal features of the late electrical fields across conditions, the main effect of site for the regression quality score, and the presence of late components induced by intracranial stimulations (e.g., Keller et al., 2018; Kunieda et al., 2015) support the idea that relevant information might be contained at such latencies.

5 | CONCLUSION

In this article, we examined the TMS intensity dependent effects on the EEG signals from a temporal and spectral perspective, and used a new analytic approach to derive regional input–output profiles of the EEG responses to TMS. We reported complex dynamical responses in three distant regions in terms of components' amplitude and oscillatory signatures. These complex properties of the local neuronal responses to TMS largely depend on the intrinsic cytoarchitecture and connectivity patterns of the stimulated area. Then, the systematic description of their intrinsic dynamical properties brings important knowledge into cortical physiology. Furthermore, our data have implication in clinical research. This new assessment of regional cortical excitability will help resolving new challenges especially in the context of pharmacological or brain stimulation induced modulations of cortical excitability (Devergnas & Wichmann, 2011; Karabanov et al., 2015; Nitsche et al., 2003). The primary motor cortex has been largely used as the experimental model to study brain reactivity to TMS and to normalize stimulation parameters when targeting nonmotor areas. Our data show that the local EEG response may be highly specific, and should not be extrapolated to other brain regions. Then using the rMT as a basis to define stimulation intensities in rTMS protocols might contribute to the large variability reported by clinical rTMS trials. Based on linear regressions, a realistic regional threshold could be derived and could serve as a basis for to set stimulation parameters at

the group level or even on an individual basis. Hence, the development of more accurate control strategies of TMS-induced changes in cortical excitability will eventually facilitate predicting the effect of rTMS applied to nonmotor brain areas.

ACKNOWLEDGMENTS

This work was funded by the Agence Nationale pour la Recherche grant "ANR-15-CE37-0015-01" and by NeuroCoG IDEX UGA in the framework of the "Investissements d'avenir" program (ANR-15-IDEX-02). Data were acquired on a platform of France Life Imaging Network partly funded by the grant "ANR-11-INBS-0006."

CONFLICT OF INTEREST

The authors declare no potential conflict of interest.

DATA AVAILABILITY STATEMENT

The data that support the findings of this study may be available from the corresponding author upon reasonable request

ORCID

Estelle Raffin https://orcid.org/0000-0003-3262-5251
Sylvain Harquel https://orcid.org/0000-0001-8756-2230
Olivier David https://orcid.org/0000-0003-0776-0216

REFERENCES

Amassian, V. E., & Cracco, R. Q. (1987). Human cerebral cortical responses to contralateral transcranial stimulation. *Neurosurgery*, *20*, 148–155.

Awiszus, F. (2003). Chapter 2 TMS and threshold hunting. In W. Paulus, F. Tergau, M. A. Nitsche, J. G. Rothwell, U. Ziemann, & M. Hallett (Eds.), *Supplements to clinical neurophysiology* (Vol. 56, pp. 13–23). Amsterdam: Elsevier Retrieved from http://www.sciencedirect.com/science/article/pii/S1567424X09702053

Badawy, R. A. B., Loetscher, T., Macdonell, R. A. L., & Brodtmann, A. (2013). Cortical excitability and neurology: Insights into the pathophysiology. *Functional Neurology*, *27*, 131–145.

Belardinelli, P., Biabani, M., Blumberger, D. M., Bortoletto, M., Casarotto, S., David, O., … Ilmoniemi, R. J. (2019). Reproducibility in TMS-EEG studies: A call for data sharing, standard procedures and effective experimental control. *Brain Stimulation*, *12*, 787–790.

Bell, A. J., & Sejnowski, T. J. (1995). An information-maximization approach to blind separation and blind deconvolution. *Neural Computation*, *7*, 1129–1159.

Biabani, M., Fornito, A., Mutanen, T. P., Morrow, J., & Rogasch, N. C. (2019). Characterizing and minimizing the contribution of sensory inputs to TMS-evoked potentials. *Brain Stimulat*, *12*, 1537–1552.

Blair, R. C., & Karniski, W. (1993). An alternative method for significance testing of waveform difference potentials. *Psychophysiology*, *30*, 518–524.

Bohning, D. E., Shastri, A., McConnell, K. A., Nahas, Z., Lorberbaum, J. P., Roberts, D. R., … George, M. S. (1999). A combined TMS/fMRI study of intensity-dependent TMS over motor cortex. *Biological Psychiatry*, *45*, 385–394.

Boroojerdi, B., Battaglia, F., Muellbacher, W., & Cohen, L. G. (2001). Mechanisms influencing stimulus-response properties of the human corticospinal system. *Clinical Neurophysiology*, *112*, 931–937.

Bortoletto, M., Veniero, D., Thut, G., & Miniussi, C. (2015). The contribution of TMS-EEG coregistration in the exploration of the human cortical connectome. *Neuroscience and Biobehavioral Reviews*, *49*, 114–124.

Brandeis, D., & Lehmann, D. (1986). Event-related potentials of the brain and cognitive processes: Approaches and applications. *Neuropsychologia*, *24*, 151–168.

Bridwell, D. A., Cavanagh, J. F., Collins, A. G. E., Nunez, M. D., Srinivasan, R., Stober, S., & Calhoun, V. D. (2018). Moving beyond ERP components: A selective review of approaches to integrate EEG and behavior. *Frontiers in Human Neuroscience*, *12*, 106.

Calhoun, V. D., Liu, J., & Adali, T. (2009). A review of group ICA for fMRI data and ICA for joint inference of imaging, genetic, and ERP data. *NeuroImage*, *45*, S163–S172.

Carota, F., Posada, A., Harquel, S., Delpuech, C., Bertrand, O., & Sirigu, A. (2010). Neural dynamics of the intention to speak. *Cerebral Cortex*, *20*, 1891–1897.

Casali, A. G., Casarotto, S., Rosanova, M., Mariotti, M., & Massimini, M. (2010). General indices to characterize the electrical response of the cerebral cortex to TMS. *NeuroImage*, *49*, 1459–1468.

Casarotto, S., Comanducci, A., Rosanova, M., Sarasso, S., Fecchio, M., Napolitani, M., … Massimini, M. (2016). Stratification of unresponsive patients by an independently validated index of brain complexity. *Ann Neurol*, *80*, 718–729.

Cash, R. F. H., Noda, Y., Zomorrodi, R., Radhu, N., Farzan, F., Rajji, T. K., … Blumberger, D. M. (2017). Characterization of glutamatergic and GABAA-mediated neurotransmission in motor and dorsolateral prefrontal cortex using paired-pulse TMS-EEG. *Neuropsychopharmacology*, *42*, 502–511.

Chervyakov, A. V., Sinitsyn, D. O., & Piradov, M. A. (2016). Variability of neuronal responses: Types and functional significance in neuroplasticity and neural Darwinism. *Frontiers in Human Neuroscience*, *10*, 603. Retrieved from https://www.ncbi.nlm.nih.gov/pmc/articles/PMC5122744/

Chung, S. W., Rogasch, N. C., Hoy, K. E., & Fitzgerald, P. B. (2015). Measuring brain stimulation induced changes in cortical properties using TMS-EEG. *Brain Stimulation*, *8*, 1010–1020.

Chung, S. W., Rogasch, N. C., Hoy, K. E., Sullivan, C. M., Cash, R. F. H., & Fitzgerald, P. B. (2018). Impact of different intensities of intermittent theta burst stimulation on the cortical properties during TMS-EEG and working memory performance. *Human Brain Mapping*, *39*, 783–802.

Conde, V., Tomasevic, L., Akopian, I., Stanek, K., Saturnino, G. B., Thielscher, A., … Siebner, H. R. (2019). The non-transcranial TMS-evoked potential is an inherent source of ambiguity in TMS-EEG studies. *NeuroImage*, *185*, 300–312.

Daskalakis, Z. J., Farzan, F., Barr, M. S., Maller, J. J., Chen, R., & Fitzgerald, P. B. (2008). Long-interval cortical inhibition from the dorsolateral prefrontal cortex: A TMS–EEG study. *Neuropsychopharmacology*, *33*, 2860–2869.

Desmurget, M., & Sirigu, A. (2012). Conscious motor intention emerges in the inferior parietal lobule. *Current Opinion in Neurobiology*, *22*, 1004–1011.

Devergnas, A., & Wichmann, T. (2011). Cortical potentials evoked by deep brain stimulation in the subthalamic area. *Frontiers in Systems Neuroscience*, *5*, 30.

Dhamne, S. C., Kothare, R. S., Yu, C., Hsieh, T.-H., Anastasio, E. M., Oberman, L., … Rotenberg, A. (2014). A measure of acoustic noise generated from transcranial magnetic stimulation coils. *Brain Stimulation*, *7*, 432–434.

Di Lazzaro, V., Oliviero, A., Meglio, M., Cioni, B., Tamburrini, G., Tonali, P., & Rothwell, J. C. (2000). Direct demonstration of the effect of lorazepam on the excitability of the human motor cortex. *Clinical Neurophysiology*, *111*, 794–799.

Di Lazzaro, V., Pilato, F., Dileone, M., Profice, P., Ranieri, F., Ricci, V., … Ziemann, U. (2007). Segregating two inhibitory circuits in human motor cortex at the level of GABAA receptor subtypes: A TMS study. *Clinical Neurophysiology*, *118*, 2207–2214.

Doron, G., & Brecht, M. (2015). What single-cell stimulation has told us about neural coding. *Philosophical Transactions of the Royal Society B*,

370, 20140204. Retrieved from https://www.ncbi.nlm.nih.gov/pmc/articles/PMC4528816/.

Farahibozorg, S.-R., Henson, R. N., & Hauk, O. (2018). Adaptive cortical parcellations for source reconstructed EEG/MEG connectomes. *NeuroImage*, *169*, 23–45.

Farzan, F., Barr, M. S., Wong, W., Chen, R., Fitzgerald, P. B., & Daskalakis, Z. J. (2009). Suppression of gamma-oscillations in the dorsolateral prefrontal cortex following long interval cortical inhibition: A TMS-EEG study. *Neuropsychopharmacology*, *34*, 1543–1551.

Farzan, F., Vernet, M., Shafi, M. M. D., Rotenberg, A., Daskalakis, Z. J., & Pascual-Leone, A. (2016). Characterizing and modulating brain circuitry through transcranial magnetic stimulation combined with electroencephalography. *Frontiers in Neural Circuits*, *10*, 73. Retrieved from http://journal.frontiersin.org/Article/10.3389/fncir.2016.00073/abstract.

Fecchio, M., Pigorini, A., Comanducci, A., Sarasso, S., Casarotto, S., Premoli, I., … Rosanova, M. (2017). The spectral features of EEG responses to transcranial magnetic stimulation of the primary motor cortex depend on the amplitude of the motor evoked potentials. *PLoS One*, *12*, e0184910.

Fernández-Ruiz, A., Muñoz, S., Sancho, M., Makarova, J., Makarov, V. A., & Herreras, O. (2013). Cytoarchitectonic and dynamic origins of giant positive local field potentials in the dentate gyrus. *The Journal of Neuroscience*, *33*, 15518–15532.

Ferreri, F., Pasqualetti, P., Määttä, S., Ponzo, D., Ferrarelli, F., Tononi, G., … Rossini, P. M. (2011). Human brain connectivity during single and paired pulse transcranial magnetic stimulation. *NeuroImage*, *54*, 90–102.

Ferreri, F., Vecchio, F., Ponzo, D., Pasqualetti, P., & Rossini, P. M. (2014). Time-varying coupling of EEG oscillations predicts excitability fluctuations in the primary motor cortex as reflected by motor evoked potentials amplitude: An EEG-TMS study. *Human Brain Mapping*, *35*, 1969–1980.

Fitzgerald, P. B., Brown, T. L., Daskalakis, Z. J., Chen, R., & Kulkarni, J. (2002). Intensity-dependent effects of 1 Hz rTMS on human corticospinal excitability. *Clin Neurophysiol Off J IntFed Clin Neurophysiol*, *113*, 1136–1141.

Fuggetta, G., Fiaschi, A., & Manganotti, P. (2005). Modulation of cortical oscillatory activities induced by varying single-pulse transcranial magnetic stimulation intensity over the left primary motor area: A combined EEG and TMS study. *NeuroImage*, *27*, 896–908.

Freedberg, M., Reeves, J. A., Hussain, S. J., Zaghloul, K. A., & Wassermann, E. M. (2020). Identifying site- and stimulation-specific TMS-evoked EEG potentials using a quantitative cosinesimilarity metric. *PloS One*, *15*, e0216185.

Gaspar, C. M., Rousselet, G. A., & Pernet, C. R. (2011). Reliability of ERP and single-trial analyses. *NeuroImage*, *58*, 620–629.

Gordon, P. C., Desideri, D., Belardinelli, P., Zrenner, C., & Ziemann, U. (2018). Comparison of cortical EEG responses to realistic sham versus real TMS of human motor cortex. *Brain Stimul Basic Transl Clin Res Neuromodulation*, *11*, 1322–1330.

Gramfort, A., Papadopoulo, T., Olivi, E., & Clerc, M. (2010). OpenMEEG: Opensource software for quasistatic bioelectromagnetics. *Biomedical Engineering Online*, *9*, 45.

Harquel, S., Bacle, T., Beynel, L., Marendaz, C., Chauvin, A., & David, O. (2016). Mapping dynamical properties of cortical microcircuits using robotized TMS and EEG: Towards functional cytoarchitectonics. *NeuroImage*, *135*, 115–124.

He, Y., Wang, J., Wang, L., Chen, Z. J., Yan, C., Yang, H., … Evans, A. C. (2009). Uncovering intrinsic modular Organization of Spontaneous Brain Activity in humans. *PLoS One*, *4*, e5226. Retrieved from https://www.ncbi.nlm.nih.gov/pmc/articles/PMC2668183/.

Hegerl, U., & Juckel, G. (1993). Intensity dependence of auditory evoked potentials as an indicator of central serotonergic neurotransmission: A new hypothesis. *Biological Psychiatry*, *33*, 173–187.

Hill, A. T., Rogasch, N. C., Fitzgerald, P. B., & Hoy, K. E. (2016). TMS-EEG: A window into the neurophysiological effects of transcranial electrical stimulation in non-motor brain regions. *Neurosci Biobehav Rev*, *64*, 175–184.

Janssen, A. M., Oostendorp, T. F., & Stegeman, D. F. (2015). The coil orientation dependency of the electric field induced by TMS for M1 and other brain areas. *Journal of NeuroEngineering and Rehabilitation*, *12*, 47.

Jeffreys, H. (1998). *The theory of probability*. Oxford, New York: OUP Oxford.

Juckel, G., Csépe, V., Molnár, M., Hegerl, U., & Karmos, G. (1996). Intensity dependence of auditory evoked potentials in behaving cats. *Electroencephalography and Clinical Neurophysiology*, *100*, 527–537.

Kähkönen, S., Komssi, S., Wilenius, J., & Ilmoniemi, R. J. (2005a). Prefrontal transcranial magnetic stimulation produces intensity-dependent EEG responses in humans. *NeuroImage*, *24*, 955–960.

Kähkönen, S., Komssi, S., Wilenius, J., & Ilmoniemi, R. J. (2005b). Prefrontal TMS produces smaller EEG responses than motor-cortex TMS: Implications for rTMS treatment in depression. *Psychopharmacology*, *181*, 16–20.

Kajikawa, Y., & Schroeder, C. E. (2011). How local is the local field potential? *Neuron*, *72*, 847–858.

Karabanov, A., Ziemann, U., Hamada, M., George, M. S., Quartarone, A., Classen, J., … Siebner, H. R. (2015). Consensus paper: Probing homeostatic plasticity of human cortex with non-invasive transcranial brain stimulation. *Brain Stimulation*, *8*, 993–1006.

Keller, C. J., Huang, Y., Herrero, J. L., Fini, M. E., Du, V., Lado, F. A., … Mehta, A. D. (2018). Induction and quantification of excitability changes in human cortical networks. *J Neurosci*, *38*, 5384–5398.

Kirschstein, T., & Köhling, R. (2009). What is the source of the EEG? *Clinical EEG and Neuroscience*, *40*, 146–149.

Komssi, S., & Kähkönen, S. (2006). The novelty value of the combined use of electroencephalography and transcranial magnetic stimulation for neuroscience research. *Brain Research Reviews*, *52*, 183–192.

Komssi, S., Kähkönen, S., & Ilmoniemi, R. J. (2004). The effect of stimulus intensity on brain responses evoked by transcranial magnetic stimulation. *Human Brain Mapping*, *21*, 154–164.

Komssi, S., Savolainen, P., Heiskala, J., & Kähkönen, S. (2007). Excitation threshold of the motor cortex estimated with transcranial magnetic stimulation electroencephalography. *Neuroreport*, *18*, 13–16.

Kujirai, T., Caramia, M. D., Rothwell, J. C., Day, B. L., Thompson, P. D., Ferbert, A., … Marsden, C. D. (1993). Corticocortical inhibition in human motor cortex. *The Journal of Physiology*, *471*, 501–519.

Kunieda, T., Yamao, Y., Kikuchi, T., & Matsumoto, R. (2015). New approach for exploring cerebral functional connectivity: Review of cortico-cortical evoked potential. *Neurol Med Chir*, *55*, 374–382.

Lea-Carnall, C. A., Montemurro, M. A., Trujillo-Barreto, N. J., Parkes, L. M., & El-Deredy, W. (2016). Cortical resonance frequencies emerge from network size and connectivity. *PLoS Computational Biology*, *12*, e1004740. Retrieved from https://www.ncbi.nlm.nih.gov/pmc/articles/PMC4767278/.

Liao, X., Cao, M., Xia, M., & He, Y. (2017). Individual differences and time-varying features of modular brain architecture. *NeuroImage*, *152*, 94–107.

Lioumis, P., Kičić, D., Savolainen, P., Mäkelä, J. P., & Kähkönen, S. (2009). Reproducibility of TMS-evoked EEG responses. *Human Brain Mapping*, *30*, 1387–1396.

Makeig, S., Bell, A. J., Jung, T. P., & Sejnowski, T. J. (1996). Independent component analysis of electroencephalographic data. *Adv Neur In*, *8*, 145–151.

Meunier, D., Lambiotte, R., & Bullmore, E. T. (2010). Modular and hierarchically modular organization of brain networks. *Frontiers in Neuroscience*, *4*, 200. Retrieved from https://www.ncbi.nlm.nih.gov/pmc/articles/PMC3000003/.

Meunier, D., Lambiotte, R., Fornito, A., Ersche, K. D., & Bullmore, E. T. (2009). Hierarchical modularity in human brain functional networks. *Frontiers in Neuroinformatics*, *3*, 37. Retrieved from https://www.ncbi.nlm.nih.gov/pmc/articles/PMC2784301/.

Möller, C., Arai, N., Lücke, J., & Ziemann, U. (2009). Hysteresis effects on the input–output curve of motor evoked potentials. *Clinical Neurophysiology*, *120*, 1003–1008.

Murakami, S., & Okada, Y. (2006). Contributions of principal neocortical neurons to magnetoencephalography and electroencephalography signals. *The Journal of Physiology*, *575*, 925–936.

Mutanen, T., Mäki, H., & Ilmoniemi, R. J. (2013). The effect of stimulus parameters on TMS-EEG muscle artifacts. *Brain Stimulation*, *6*, 371–376.

Nakamura, H., Kitagawa, H., Kawaguchi, Y., & Tsuji, H. (1996). Direct and indirect activation of human corticospinal neurons by transcranial magnetic and electrical stimulation. *Neuroscience Letters*, *210*, 45–48.

Nettekoven, C., Volz, L. J., Kutscha, M., Pool, E.-M., Rehme, A. K., Eickhoff, S. B., … Grefkes, C. (2014). Dose-dependent effects of theta burst rTMS on cortical excitability and resting-state connectivity of the human motor system. *J Neurosci*, *34*, 6849–6859.

Nitsche, M. A., Liebetanz, D., Antal, A., Lang, N., Tergau, F., & Paulus, W. (2003). Modulation of cortical excitability by weak direct current stimulation—technical, safety and functional aspects. *Supplements to Clinical Neurophysiology*, *56*, 255–276.

Oostenveld, R., Fries, P., Maris, E., & Schoffelen, J.-M. (2011). FieldTrip: Open source software for advanced analysis of MEG, EEG, and invasive electrophysiological data. *Computational Intelligence and Neuroscience*, *2011*, 156869.

Opie, G. M., Rogasch, N. C., Goldsworthy, M. R., Ridding, M. C., & Semmler, J. G. (2017). Investigating TMS-EEG indices of long-interval intracortical inhibition at different interstimulus intervals. *Brain Stimulation*, *10*, 65–74.

Paus, T., Sipila, P. K., & Strafella, A. P. (2001). Synchronization of neuronal activity in the human primary motor cortex by transcranial magnetic stimulation: An EEG study. *Journal of Neurophysiology*, *86*, 1983–1990.

Petrichella, S., Johnson, N., & He, B. (2017). The influence of corticospinal activity on TMS-evoked activity and connectivity in healthy subjects: A TMS-EEG study. *PLoS One*, 12, e0174879. Retrieved from https://www.ncbi.nlm.nih.gov/pmc/articles/PMC5383066/.

Premoli, I., Király, J., Müller-Dahlhaus, F., Zipser, C. M., Rossini, P., Zrenner, C., … Belardinelli, P. (2018). Short-interval and long-interval intracortical inhibition of TMS-evoked EEG potentials. *Brain Stimulation*, *11*, 818–827.

Premoli, I., Rivolta, D., Espenhahn, S., Castellanos, N., Belardinelli, P., Ziemann, U., & Müller-Dahlhaus, F. (2014). Characterization of GABAB-receptor mediated neurotransmission in the human cortex by paired-pulse TMS-EEG. *NeuroImage*, *103*, 152–162.

Reuter, M., Schmansky, N. J., Rosas, H. D., & Fischl, B. (2012). Within-subject template estimation for unbiased longitudinal image analysis. *NeuroImage*, *61*, 1402–1418.

Ridding, M. C., & Rothwell, J. C. (1997). Stimulus/response curves as a method of measuring motor cortical excitability in man. *Electroencephalography and Clinical Neurophysiology*, *105*, 340–344.

Rogasch, N. C., Daskalakis, Z. J., & Fitzgerald, P. B. (2013). Mechanisms underlying long-interval cortical inhibition in the human motor cortex: A TMS-EEG study. *Journal of Neurophysiology*, *109*, 89–98.

Rogasch, N. C., Daskalakis, Z. J., & Fitzgerald, P. B. (2015). Cortical inhibition of distinct mechanisms in the dorsolateral prefrontal cortex is related to working memory performance: A TMS-EEG study. *Cortex*, *64*, 68–77.

Rogasch, N. C., & Fitzgerald, P. B. (2013). Assessing cortical network properties using TMS-EEG. *Human Brain Mapping*, *34*, 1652–1669.

Rogasch, N. C., Thomson, R. H., Farzan, F., Fitzgibbon, B. M., Bailey, N. W., Hernandez-Pavon, J. C., … Fitzgerald, P. B. (2014). Removing artefacts from TMS-EEG recordings using independent component analysis: Importance for assessing prefrontal and motor cortex network properties. *NeuroImage*, *101*, 425–439.

Rosanova, M., Casali, A., Bellina, V., Resta, F., Mariotti, M., & Massimini, M. (2009). Natural frequencies of human corticothalamic circuits. *The Journal of Neuroscience*, *29*, 7679–7685.

Rossini, P. M., Burke, D., Chen, R., Cohen, L. G., Daskalakis, Z., Di Iorio, R., … Ziemann, U. (2015). Non-invasive electrical and magnetic stimulation of the brain, spinal cord, roots and peripheral nerves: Basic principles and procedures for routine clinical and research application. An updated report from an I.F.C.N. committee. *Clinical Neurophysiology*, *126*, 1071–1107.

Sabate, M., Llanos, C., Enriquez, E., & Rodriguez, M. (2012). Mu rhythm, visual processing and motor control. *Clinical Neurophysiology*, *123*, 550–557.

Salustri, C., Tecchio, F., Zappasodi, F., Bevacqua, G., Fontana, M., Ercolani, M., … Rossini, P. M. (2007). Cortical excitability and rest activity properties in patients with depression. *Journal of Psychiatry & Neuroscience*, *32*, 259–266.

Saari, J., Kallioniemi, E., Tarvainen, M., & Julkunen, P. (2018). Oscillatory TMS-EEG-responses as a measure of the cortical excitability threshold. *IEEE Trans Neural Syst Rehabil Eng*, *26*, 383–391.

Shiga, Y., Yamada, T., Ofuji, A., Fujita, Y., Kawamura, T., Inoue, K., … Yeh, M. H. (2016). Effects of stimulus intensity on latency and conduction time of short-latency somatosensory evoked potentials. *Clinical electroencephalography*, *32*, 75–81. Retrieved from https://journals.sagepub.com/doi/10.1177/155005940103200206.

Siebner, H. R., Conde, V., Tomasevic, L., Thielscher, A., & Bergmann, T. O. (2019). Distilling the essence of TMS-evoked EEG potentials (TEPs): A call for securing mechanistic specificity and experimental rigor. *Brain Stimulation*, *12*(4), P1051–P1054.

Smith, J. E., & Peterchev, A. V. (2018). Electric field measurement of two commercial active/sham coils for transcranial magnetic stimulation. *Journal of Neural Engineering*, *15*, 054001.

Stokes, M. G., Chambers, C. D., Gould, I. C., English, T., McNaught, E., McDonald, O., & Mattingley, J. B. (2007). Distance-adjusted motor threshold for transcranial magnetic stimulation. *Clinical Neurophysiology*, *118*, 1617–1625.

Sur, S., & Sinha, V. K. (2009). Event-related potential: An overview. *Industrial Psychiatry Journal*, *18*, 70–73.

Tadel, F., Baillet, S., Mosher, J. C., Pantazis, D., & Leahy, R. M. (2011). Brainstorm: A user-friendly application for MEG/EEG analysis. *Computational Intelligence and Neuroscience*, *2011*, 879716.

ter Braack, E. M., deVos, C. C., & van Putten, M. J. A. M. (2015). Masking the auditory evoked potential in TMS-EEG: A comparison of various methods. *Brain Topogr*, *28*, 520–528.

Tiwari, V., Ambadipudi, S., & Patel, A. B. (2013). Glutamatergic and GABAergic TCA cycle and neurotransmitter cycling fluxes in different regions of mouse brain. *Journal of Cerebral Blood Flow and Metabolism*, *33*, 1523–1531.

Trebaul, L., Deman, P., Tuyisenge, V., Jedynak, M., Hugues, E., Rudrauf, D., … David, O. (2018). Probabilistic functional tractography of the human cortex revisited. *NeuroImage*, *181*, 414–429.

Tsuji, S., Lüders, H., Dinner, D. S., Lesser, R. P., & Klem, G. (1984). Effect of stimulus intensity on subcortical and cortical somatosensory evoked potentials by posterior tibial nerve stimulation. *Electroencephalography*, *59*, 229–237.

Veniero, D., Bortoletto, M., & Miniussi, C. (2014). On the challenge of measuring direct cortical reactivity by TMS-EEG. *Brain Stimulation*, *7*, 759–760.

Yi, G.-S., Wang, J., Tsang, K.-M., Wei, X.-L., & Deng, B. (2015). Input-output relation and energy efficiency in the neuron with different spike threshold dynamics. *Frontiers in Computational Neuroscience*, *9*, 62.

Ziemann, U., Rothwell, J. C., & Ridding, M. C. (1996). Interaction between intracortical inhibition and facilitation in human motor cortex. *The Journal of Physiology*, *496*(Pt 3), 873–881.

Ziemann, U., Reis, J., Schwenkreis, P., Rosanova, M., Strafella, A., Badawy, R., & Müller-Dahlhaus, F. (2015). TMS and drugs revisited 2014. *Clinical Neurophysiology*, *126*(10), 1847–1868 Retrieved from https://www.ncbi.nlm.nih.gov/pubmed/25534482.

SUPPORTING INFORMATION

Additional supporting information may be found online in the Supporting Information section at the end of this article.

How to cite this article: Raffin E, Harquel S, Passera B, Chauvin A, Bougerol T, David O. Probing regional cortical excitability via input–output properties using transcranial magnetic stimulation and electroencephalography coupling. *Hum Brain Mapp*. 2020;41:2741–2761. https://doi.org/10.1002/hbm.24975